Extracellular vesicles to evaluate the effects of mesenchymal stromal cells in the premature lung

Mairéad Green

A thesis submitted to the University of Ottawa in partial fulfillment of the requirements for the Master's degree in Cellular and Molecular Medicine

Department of Cellular and Molecular Medicine
Faculty of Medicine
University of Ottawa

Abstract

Bronchopulmonary dysplasia (BPD), caused by disrupted lung development, is a common complication of prematurity without effective treatment. Mesenchymal stromal cells (MSCs) improve features of experimental BPD, such as lung function, structure, and inflammation. The HULC-1 trial assessed the safety of MSCs for BPD. Since MSC mechanisms in the premature lung remain unclear, we hypothesized that extracellular vesicles (EVs) might reflect MSC effects. We analyzed EVs from tracheal aspirates (TA) collected before and after MSC treatment using two flow cytometry methods: antibody-capture to identify cellular origin and single particle analysis to quantify EVs. TA-EVs primarily originated from lung epithelium and immune cells. After MSC administration, total TA-EVs increased threefold within 3–4 days, though EVs from specific cell types showed no significant change. This suggests the EV increase may not be cell-type-specific. These findings highlight TA-EVs as potential biomarkers for MSC treatment response in preterm infants, warranting further investigation.

Abbreviations

a.u	Arbitrary units
AF488	AlexaFluor 488
APC	Allophycocyanin
ARDS	Acute respiratory distress syndrome
AT1	Type 1 alveolar epithelial cell
AT2	Type 2 alveolar epithelial cell
BALF	Bronchoalveolar lavage fluid
BPD	Bronchopulmonary dysplasia
CFSE	Carboxyfluorescein succinimidyl ester
CLD	Chronic lung disease
CMG	CellMask Green
CNN	Canadian Neonatal Network
COPD	Chronic obstructive pulmonary disease
DOL	Day of life
ERF	Equivalent reference fluorophore
EV	Extracellular vesicle
FiO_2	Fraction of inspired oxygen
FITC	Fluorescein isothiocyanate
hUC-MSC	Human umbilical cord derived mesenchymal stromal cell
HULC-1	Helping Underdeveloped Lungs with Cells-1
HULC-Obs	Helping Underdeveloped Lungs with Cells-Observational
IL-6	Interleukin-6
IL-8	Interleukin-8
IL-10	Interleukin-10
IPF	Idiopathic pulmonary fibrosis
MESF	Molecules of equivalent soluble fluorophore
MFI	Median fluorescence intensity
MMP-9	Matrix metalloproteinase 9
MSC	Mesenchymal stromal cell
nFC	Nanoflow cytometry
NTA	Nanoparticle tracking analysis
PBS	Phosphate buffered saline
PE	Phycoerythrin
PMA	Postmenstrual age
RDS	Respiratory distress syndrome
SAE	Severe adverse event
TA	Tracheal aspirate
TA-EV	Tracheal aspirate extracellular vesicle
TEM	Transmission electron microscopy
TGB-β	Transforming growth factor beta
TNF-α	Tumour necrosis factor alpha
UC	Umbilical cord
UCB	Umbilical cord blood
uEV	Urine extracellular vesicle

Table of contents

List of figures

List of tables

Appendices

Acknowledgements

I would like to thank my supervisor, Dr. Bernard Thébaud, for the opportunity to conduct my Master's research in his lab, and for providing me with guidance and support during my studies. I would also like to thank all the members of the Thébaud lab who helped me in my work: Dr. Chanèle Cyr-Depauw, Dr. Ewa Henckel, Celine Fawagreh, Shumei Zhong, Cari Bai, Mahnaz Nazari, Sahar Salari, Adithya Achutan, Doreen Engelberts, Dr. Wojciech Durlak, Dr. Arul Vadivel, Dr. Liqun Xu and Dr. Marc-Olivier Desguise. Thank you also to Chantal Horth, Becky Grimwood, and Viviane Olsen for their support in this project.

I would like to express my gratitude to Dr. Ewa Henckel, who took me under her wing and was always there to offer me encouragement and guidance (as well as a fika). I am thankful to have worked with you and grateful to call you my friend.

Thank you to my thesis advisory committee members, Drs. Dylan Burger and Vera Tang, for their invaluable knowledge and expertise in producing this work. Thank you to Drs. Vera Tang and Manoj Lalu for agreeing to evaluate this thesis.

I would also like to thank my parents for their support and for encouraging me to further my studies. Thank you to my best friends, Angie and Elie, for supporting me and always asking about my work. And lastly, thank you to my guinea pig Angelica, who sat with me for many hours of data analysis and writing.

1. Introduction

1.1 Bronchopulmonary dysplasia

Bronchopulmonary dysplasia (BPD) is a chronic lung disease of prematurity. First characterized in 1967, the condition occurred in modestly premature infants receiving mechanical ventilation with high concentrations of oxygen, and was characterized by scarring and fibrosis of the lung (1). BPD has now evolved into a new phenotype due to the advent of surfactant and other improvements in the care of neonatal infants. The hallmarks of "new" BPD include alveolar and microvascular simplification, which, when combined with inflammation, result in alterations to both lung structure and function.

1.1.1 Epidemiology

Prematurity is defined as birth before 37 weeks' gestation. In Canada, ~30,000 babies are born premature every year, representing approximately 8-10% of all births (2). In 2023, across 33 sites participating in the Canadian Neonatal Network (CNN), 1,191 infants were born before 28 weeks, which is considered extremely preterm birth (3). Infants born as early as 23 and 24 weeks are increasingly surviving, thanks to advances in neonatal care, however they frequently experience major neonatal morbidities, such as necrotizing enterocolitis, retinopathy of prematurity, and BPD (4). BPD is the most common complication of prematurity, affecting approximately 35% of at-risk infants (5). Diagnosis of BPD typically occurs at 36 weeks post-menstrual age (PMA, refers to the gestational age plus chronological age of the infant), and is based on the level of respiratory support required by the infant.

1.1.2 Interrupted lung development

Lung development in humans occurs in five stages, beginning during the embryonic period and ending in early adulthood (summarized in Figure 1, adapted from refs (6,7)). During the embryonic stage (weeks 3-6), major structures of the lung like the trachea, main bronchi and lobes appear. Airways are then formed by branching morphogenesis in the pseudoglandular stage (6-16 weeks). This is followed by formation of the saccules, which are precursors to the gas exchange units of the lung, during the

canalicular period (16-26 weeks). It is at this time that respiratory epithelium begins to differentiate into type 2 (AT2) and type 1 (AT1) alveolar epithelial cells, and the first air-blood barriers form (8). AT1 are thin cells that allow gas exchange, and AT2 will eventually produce surfactant proteins to prevent alveolar collapse. AT2 are also the progenitor cells in the lung: upon injury to AT1 cells, AT2 transdifferentiate into AT1 cells. Septation of the saccules occurs during the saccular stage (26-36 weeks), during which the surface area for gas exchange increases, and AT2 and AT1 cells mature. Endothelial cells begin joining to AT1 cells, to allow efficient gas exchange (9). Alveolar endothelium is composed of general capillary endothelial cells (gCap or Cap 1), which are involved in capillary regeneration, and aerocytes (aCap or Cap 2), which participate in gas exchange. Septation and maturation continue from 37 weeks until early adulthood (10).

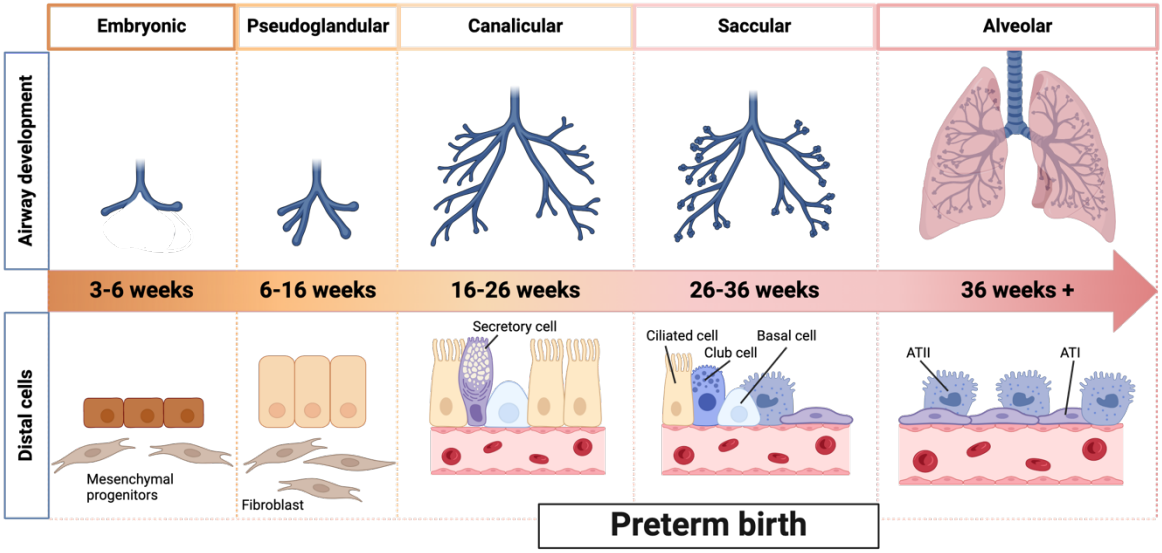

Figure 1. Fetal lung development from the embryonic to alveolar stages. Adapted from refs (6,7).

Premature birth occurs during the late canalicular (weeks 22-26) and saccular (weeks 26-36) stages of lung development. Especially at earlier weeks, septation has not produced sufficient surface area for efficient gas exchange, and AT2 cells have not matured enough to produce adequate surfactant to prevent alveolar collapse. Furthermore, the microvascular network has not significantly developed to support gas exchange (11). These shortcomings cause premature infants to develop respiratory distress

syndrome (RDS) at birth, which requires medical interventions for the survival of the infant. Further development of the lung to the alveolar stage is therefore interrupted, leading to structural abnormalities, resulting in BPD.

1.1.3 Pathophysiology

BPD is a multifactorial disease originating from several pre- and post-natal insults. Antenatally, maternal smoking, intrauterine growth restriction, and chorioamnionitis have all been associated with the development of the condition (12–16). On the other hand, postnatal insults often arise from medical interventions necessary for the survival of the infant, in combination with other complications of prematurity, such as sepsis (17).

As explained in the previous section, premature infants frequently receive supplemental oxygen and mechanical ventilation due to RDS. In response to these interventions, alveolar cells release pro-inflammatory cytokines such as interleukin-6 (IL-6) and tumor necrosis factor-alpha (TNF-a), causing infiltration of neutrophils. Through degranulation, neutrophils release injurious metalloproteinases and elastases, further damaging lung tissue (18–21). This is followed by an influx of monocytes, which differentiate into pro-inflammatory macrophages (M1). M1 macrophages attract additional inflammatory cells, causing the release of more pro-inflammatory factors, and thus contributing to inflammation in BPD (22).

Moreover, the activation of macrophages and neutrophils leads to the release of reactive oxygen species (ROS), which damage proteins, nucleic acids, and lipids, eventually resulting in cell death and inactivation of surfactant (23). As the antioxidant defence system of premature infants is not yet fully developed, the result is an imbalance of pro- and antioxidants, leading to oxidative stress (OS) (24–26). OS increases the permeability of capillaries, facilitating the passage of cytokines into the alveolar space which promotes further inflammation (27).

Beyond inflammation, hyperoxia leads to dysfunction of the alveolar cells. Hou *et al*. established that there is increased transdifferentiation of AT2 to AT1 in response to hyperoxia, suggesting a

compensatory mechanism to replace AT1 lost to injury. However, transdifferentiation did not repair injury to the lung, as structural and functional changes to both AT1 and AT2, as well as the blood-air barrier, were observed (28). Increased mRNA of AT1 marker genes HOPX and PDPN were also noted by Xia *et al.* when human neonatal alveolar cells were exposed to hyperoxia for 48 hours, suggesting that hyperoxia led to transdifferentiation (29). The injury to the cells appears to persist long-term: a small study examining lung tissue of one-year-old infants diagnosed with BPD and experiencing persistent clinical respiratory symptoms showed decreased expression of AT1 markers and mRNA. In terms of endothelial cells, hyperoxia led to reduction of gCap cells and increase of aCap cells compared to normoxia, suggesting decreased repair capacity (30). As pulmonary vascularization has been demonstrated to be necessary for proper alveolarization (31), this finding may have implications for the alveolar simplification seen in infants with BPD.

Thus, BPD results from interruption of lung development at a structural and cellular level, due to antenatal and postnatal factors as well as premature birth itself. The chronic nature of this disease has implications for the long-term health of these infants.

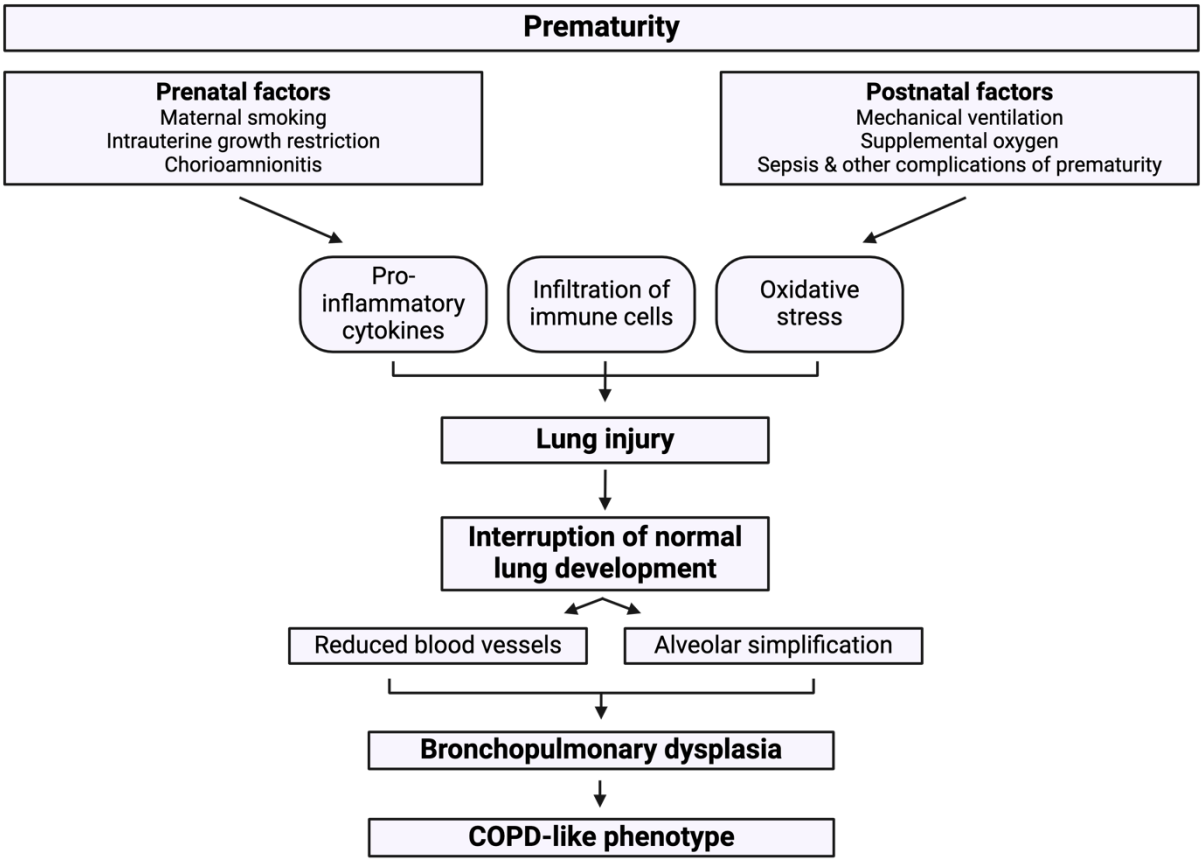

Figure 2. Summary of events involved in the pathogenesis of BPD.

1.1.4 Long term consequences of prematurity

Advances in neonatal care over the past decades mean that premature infants are now reaching adulthood. Survivors of extreme prematurity face long term consequences across organ systems, such as neurodevelopmental disabilities (32), visual impairment (33), and cardiac and renal disease (34), to name a few. By far the most studied long-term effects of extreme prematurity are respiratory consequences, which often continue well into adulthood.

Both imaging and lung function tests have been used to assess the quality of respiratory health in survivors of prematurity. Imaging studies suggest that the interruption of lung development leads to abnormalities in alveolar structure that persist in adolescence and adulthood (35–37). Particularly, the presence of enlarged alveoli is concerning for the development of an emphysema-like phenotype. Indeed, survivors of prematurity tend to have airway obstruction (38,39), suggesting that a chronic obstructive pulmonary disease (COPD)-like disease may develop later on in life. The lack of improvement of indices of respiratory health following survival of prematurity demonstrates that while current care allows these

infants to survive, there is a need to develop more effective treatments so that they can lead more healthy lives. One such promising treatment avenue is cellular therapy using mesenchymal stromal cells (MSCs).

1.2 Mesenchymal stromal cells

MSCs are multipotent progenitor cells that can be isolated from tissues such as bone marrow, adipose tissue, and umbilical cord (UC). The International Society for Cell & Gene Therapy (ISCT) defines MSCs as being plastic adherent, having the ability to differentiate to chondrocytes, osteoblasts, and adipocytes in vitro, and by the presence of CD73, CD90 and CD105, and absence of CD45 (40). These cells have regenerative and anti-inflammatory effects in several diseases and have been studied as therapeutics for BPD and other respiratory illnesses.

1.2.1 MSCs for BPD

The safety and therapeutic effect of MSCs have been established in many preclinical lung disease models including in BPD. Hyperoxia-exposed animals that received MSCs had decreased alveolar simplification, lung inflammation, pulmonary hypertension, fibrosis, and apoptosis, as well as increased angiogenesis compared to non-treated hyperoxia exposed animals (41). At 6 months post-MSC treatment, improved lung histology was sustained, and exercise capacity was improved compared to untreated hyperoxia-exposed rats, providing evidence for the long-term effectiveness of the treatment. Additionally, no tumours were detected when treated rats underwent CT scanning, demonstrating the safety of MSCs in rats up to 6 months.

1.2.1.2 Clinical trials of MSCs for BPD

The positive results obtained from preclinical studies have allowed early phase clinical trials of MSCs for the prevention of BPD to take place. To date, three Phase I and one Phase II trials have published their results (summarized in **Table 1**). Phase I trials are small and test the safety of a therapy, whereas in Phase II studies, efficacy may be tested in a larger cohort. In the three available Phase I studies, no severe adverse events (SAE) were associated with MSCs, and all concluded that MSCs are a

safe intervention for extremely preterm infants (42–44). Two year follow-ups were available for two of the studies, and no SAE associated with MSCs were reported, indicating safety up to two years (42,43).

Table 1. Summary of clinical trials studying UC-MSCs for the prevention of BPD with published results.

Trial ID	Location	Phase	Dose (cells/kg)	Administration	Year	Reference
NCT01297205	South Korea	I	10 million (n=3), 20 million (n=6)	Intratracheal	2014	(45)
NCT01828957	South Korea	II	10 million (n=33)	Intratracheal	2021	(46)
NCT02381366	United States	I	10 million (n=6), 20 million (n=6)	Intratracheal	2019	(44)
NCT02443961	Spain	I	3 doses of 5 million	Intravenous	2024	(42)

Year refers to year of study publication.

Secondary outcome measures of Phase I trials included incidence and severity of BPD, occurrence of complications of prematurity, and inflammatory biomarkers in blood and tracheal aspirate (TA). In the South Korean study (45), the severity of BPD was significantly lower in the human umbilical cord MSCs (hUC-MSCs)-treated group than the historical case-matched comparison group. The American (44) and Spanish (42) groups, however, did not find a difference in BPD severity. MSCs also appeared to mediate inflammation, as IL-6, IL-8, TNF-a, and TGF-b measured in TA were significantly lower 7 days after treatment compared to 3 days after treatment in the South Korean study. Similarly, the Spanish study reported that IL-6 in serum and bronchoalveolar lavage fluid (BALF) trended lower after treatment with the cells, suggesting improvement of inflammation. The American study did not look at biomarkers of inflammation. These encouraging results demonstrate the potential short-term benefits of MSCs for BPD.

At two year follow-up, the South Korean group did not observe long term respiratory complications typical of BPD (43), nor any differences in complications of prematurity between a treated and an untreated comparison group. Similar numbers of infants in each group were discharged home on supplemental oxygen in the Spanish group (42). Of note, the American study did not publish findings from any follow-ups. Both the South Korean and the Spanish studies led to Phase II trials, one of which is still being conducted, and results are therefore not available.

The South Korean group completed their Phase II study and published their initial (46) and five year follow-up results (47). This study enrolled 33 patients each in a treatment and a control group. Significant improvement in BPD severity and mortality were not demonstrated in infants born between 23 and 28 weeks. Subgroup analysis, however, did show that MSCs significantly improved the severity of BPD in infants born at 23 or 24 weeks compared to untreated controls. TA inflammatory cytokines IL-1b, IL-6, IL-8, TNF-a, TGF-b and MMP-9 were all significantly lower 7 days after treatment compared to the control group, indicating some anti-inflammatory effects of the cells. Follow-up at five years showed that MSCs tended to improve the respiratory morbidity of these infants, although it was not statistically significant. This is thought to be due to small sample size, rendering the study power insufficient to detect significant changes.

Our group recently completed Helping Underdeveloped Lungs with Cells-1 (HULC-1) a Phase I, dose escalation clinical trial of the safety and feasibility of umbilical cord derived MSCs for extremely preterm infants at risk of developing BPD (NCT04255147). HULC-1 was preceded by an observational study, hereafter referred to as HULC-Obs, the purpose of which was to refine the trial protocol prior to undertaking an interventional clinical trial. A Phase II trial, HULC-2, is currently being prepared.

These trials highlight the promise of MSCs for BPD, although they still have a long path to regular clinical use.

1.2.3 Mechanisms of action of MSCs

Despite advances in the therapeutic use of MSCs, the mechanism of action of these cells in attenuating lung injury associated with prematurity is incompletely understood. MSCs do not engraft in the lung, but rather act on resident lung cells in a paracrine fashion to regenerate and decrease inflammation seen in BPD (48). It is known that MSCs and their conditioned media are associated with decreases in pro-inflammatory cytokines like IL-6 and TNF-a and increases in anti-inflammatory cytokines like IL-10. Németh *et al.* reported that MSCs modulated macrophages via secretion of

prostaglandin E2, which has been corroborated by other groups (49,50). Another group studying MSC derived particles determined that hepatocyte growth factor (HGF) was responsible for improving endothelial cell permeability, leading to decreased endothelial cell apoptosis and increased proliferation (51). Loss of HGF by knockdown diminished the therapeutic effect of the particles. Similarly, a group investigating vascular endothelial growth factor (VEGF) found that knockdown of the compound led to loss of therapeutic effects from MSC derived therapies (52,53). TNF-stimulated gene 6 (TSG-6), identified in the conditioned media of MSCs, has also been found to have a role in regulation of lung inflammation caused by hyperoxia (54). These studies highlight that MSCs act via modulation of several different pathways. This is one of their advantages over studying pharmaceutical drugs for BPD, which may only target one pathway.

MSCs may also interact directly with immune cells to produce their therapeutic effects. In a mouse model of BPD, uptake of MSC-EVs by alveolar macrophages reduced gene expression of typical proinflammatory macrophage (M1) markers *Tnfa*, *Il6*, and *Ccl5* (50). In a later study, the same group demonstrated that MSC-EVs are taken up by CD45+, CD11b+, CD64+ and F4/80+ myeloid cells in the lung, promoting an M2-like macrophage phenotype and initiating resolution of lung injury (55).

Although these and other studies provide valuable information on possible mechanisms by which MSCs exert their therapeutic effects, the exact interactions between MSCs and cells of the premature lung remain elusive. Recently, extracellular vesicles (EVs) have been investigated as mediators of cellular communication that may carry keys to better understand MSC treatment.

1.3 Extracellular vesicles

1.3.1 Biology of extracellular vesicles

Cells secrete and shed membrane-enveloped nanoparticles broadly referred to as extracellular vesicles (EVs). Initially, EVs were thought to be carriers of unwanted cellular material (56), although more recent studies have identified that they play a role in intercellular signalling, homeostasis, and

pathology. The renewed interest in EVs has generated large numbers of studies focusing on their biogenesis, function, and clinical translation as biomarkers or therapeutics.

EVs are mostly created by two major pathways: the endocytic pathway, which produces exosomes, and budding directly from the cell membrane to produce ectosomes (57). Other mechanisms, such as apoptosis, may also generate specific EV subtypes. In the endocytic pathway, inward blebbing of the plasma membrane forms early endosomes, which will mature into late endosomes. Intraluminal vesicles (ILV) are formed by inward budding of the membrane of late endosomes, generating a multivesicular body (MVB). The MVB is either targeted to the lysosome for degradation, or it fuses with the cell's plasma membrane, releasing exosomes into the extracellular space (58,59). On the other hand, ectosomes are formed by outwards budding of the plasma membrane, which is then pinched off, releasing the vesicle (60,61). This process involves cytoskeletal elements, such as actin, as well as rearrangement of phospholipids, like externalization of phosphatidylserine.

During biogenesis, extracellular vesicles produced by both pathways acquire soluble and membrane proteins. Microdomains composed of lipids and membrane proteins assemble at either the limiting membrane of the MVB, or at the cell's plasma membrane. These microdomains, also called tetraspanin enriched microdomains, recruit soluble proteins and other membrane proteins which will become the cargo of the EV (62). Microdomains may also serve to promote membrane curvature, which is followed by the budding and pinching required for EV release (63).

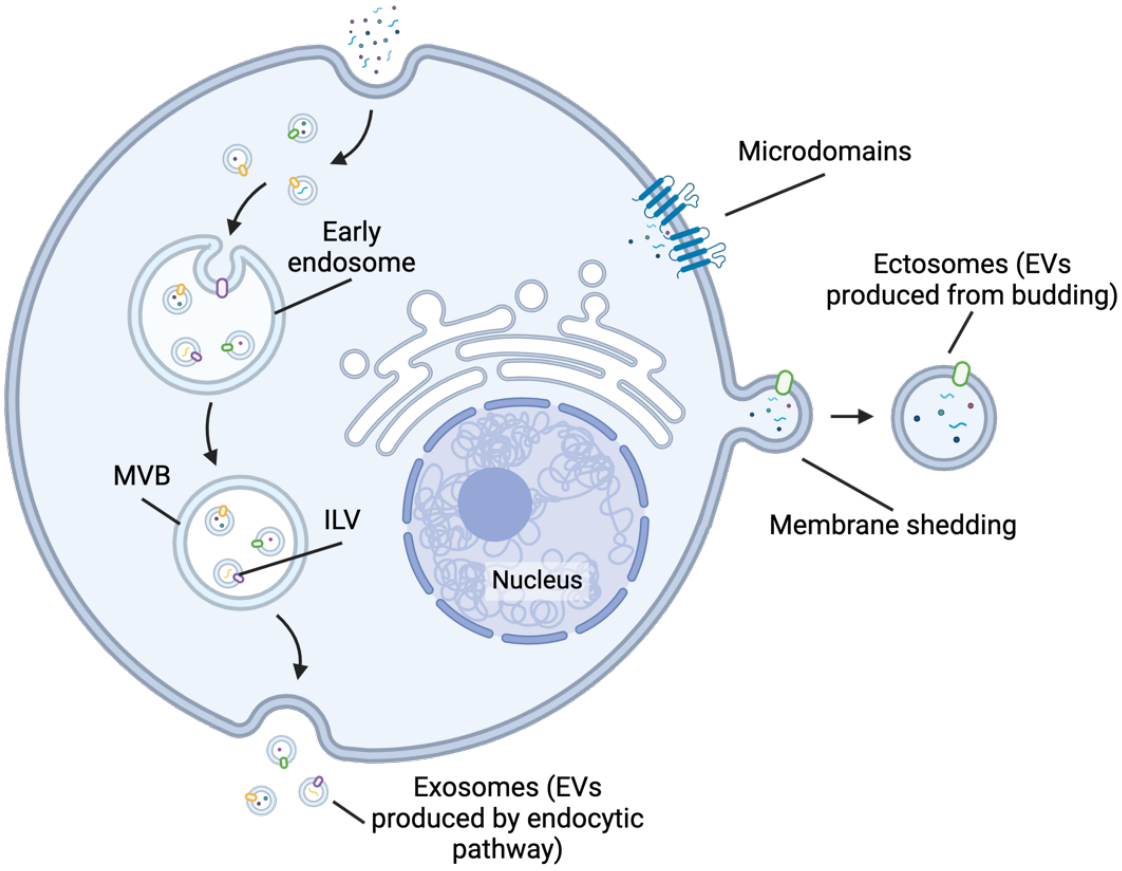

Figure 3. Major biogenesis pathways of extracellular vesicles (EVs). *MVB, multivesicular body. ILV, intraluminal vesicle.*

In the extracellular space, EVs can trigger a phenotypic or physiologic change in recipient cells through binding or delivery of their content. The surface markers of EVs, as well as soluble proteins contained in the EV corona, bind to receptors on the cell surface to initiate a change. EVs may initiate these changes by directly binding to the cell, without delivery of their contents. For example, in fibrotic lung disease, fibronectin at the surface of fibroblast-derived EVs binds to integrin α5β1 of adjacent lung fibroblasts. The binding event activates focal adhesion kinase and Src kinases to induce migration and invasion of the cells (64). More commonly, EVs bind to the cell, triggering their endocytosis or fusion to the plasma membrane, which allows delivery of their molecular contents. This is illustrated by delivery of alveolar macrophage EVs containing suppressor of cytokine signalling 3 (SOCS3) protein to alveolar epithelial cells. Uptake of this protein via EVs inhibited JAK-STAT signalling in the receiving cell, resulting in dampening of inflammation (65,66).

The cargo and surface markers of EVs reflect their cell of origin, which has implications for the study of disease-specific biomarkers and functional roles of EVs in pathological states (67). Cells exposed

to insults, for example to hyperoxia and mechanical stretch, have altered EV secretion and cargo. Human pulmonary artery endothelial cells exposed to 18% cyclic stretch (CS), which mimics mechanical ventilation, released markedly more EVs than cells not exposed to CS (68). Compared to EVs from cells not exposed to CS, these EVs contained unique proteins that are enriched in pathways related to acute respiratory distress syndrome, such as endothelial cell barrier function. Indeed, when these EVs were injected into healthy mice, the animals displayed increased inflammatory cell counts in BALF compared to animals who received phosphate buffered saline (PBS), suggesting an inflammatory effect in the lung. This study demonstrates that exposure of cells to harmful stimuli alters the cargo of their released EVs, which further promotes the pathological state.

1.3.2 EVs in lung disease

To this end, EVs have been studied to better understand the development of lung disease. They are released from a variety of lung cell types, including epithelial cells, alveolar macrophages, monocytes, neutrophils, and endothelial cells. EVs have been of particular interest in lung diseases as many lack appropriate and specific biomarkers. Additionally, the pathophysiology of many lung diseases is incompletely understood, and EVs have the potential to elucidate some of the mechanisms of disease. EVs in the lung have been explored in acute respiratory distress syndrome (ARDS, (69)), sepsis (70), chronic obstructive pulmonary disease (COPD, (71,72)) and idiopathic pulmonary fibrosis (IPF, (73)), among others. These studies will be further discussed in **Section 1.3.4**, with a focus on the technical aspect of the research.

EVs may be isolated from various biofluids to gain insight into mechanisms of action of disease. For adult lung disease, blood and bronchoalveolar lavage fluid (BALF) have been used as sources of EVs. Both sample types are generally available in large enough quantities for EV analysis. However, in premature infants, the collection of samples for EV analysis is more difficult. Considering that premature infants are estimated to have a blood volume of around 85 mL/kg, the smallest premature infants could have as little as 50 mL of blood (74,75). Furthermore, blood loss in this patient population due to

phlebotomy is significant (76). Therefore, for premature infants, it may be more beneficial to study EVs from tracheal aspirates (TA). TA are respiratory secretions collected during routine care of intubated premature infants, making them easily accessible and more representative of the lungs than other sources, like urine.

1.3.3 EVs in BPD

Only five studies have examined EVs from tracheal aspirates, all in the context of BPD. The first such study occurred in 2016: after identifying mast cells as contributors to alveolar simplification in a mouse model of neonatal chronic lung disease (CLD), Veerappan and colleagues aimed to assess the usefulness of mast cell products, including exosomes, as biomarkers of CLD (77). To demonstrate that mast cells were contributors to the TA exosome population, mast cell specific transcripts CPA3 and TPSAB1 were detected in exosomes from TA of preterm infants with CLD (n=4). Mass spectrometry and Western blot identified mast cell proteases like chymase and carboxypeptidase A3 in exosomes from supernatants of cultured human mastocytoma cells. However, mass spectrometry did not detect these proteins in preterm infant TA exosomes, and western blot was not conducted. While this study does not provide convincing evidence for the presence of mast cell exosomes in TA, it is the first to present evidence of TA-EVs in this patient population.

Next, Lal *et al.* aimed to identify exosomal miRNA at birth that could predict the development of severe BPD at 36 weeks PMA (78). Differentially expressed exosomal miRNAs between a BPD-resistant and BPD-susceptible group revealed that low exosomal miR 876-3p was the most sensitive predictor of severe BPD. In both in vitro and in vivo models of BPD, gain of function of miR 876-3p rescued alveolarization and reduced inflammation. Little is known about miR 876-3p, especially with regards to prematurity, although it appears to regulate glucose homeostasis and cancer metastasis (79,80). Despite this finding, the mechanism of miR 876-3p in preventing neonatal lung injury has not been further explored.

As part of a study focused on COPD, Genschmer and colleagues investigated the pathogenicity of EVs from activated neutrophils in TA (81). After confirming that CD66b+ EVs from humans with COPD led to a COPD phenotype in mice, EVs from TA of intubated infants with and without BPD were adoptively transferred to test the generalizability of the findings across lung disease. Neutrophil EVs from TA of BPD patients led to the alveolar simplification characteristic of the condition, suggesting that EVs have a functional role in lung disease.

Lastly, Ransom *et al.* aimed to elucidate the relationship between EVs in TA and lung development (82). They used a bead-based flow cytometry approach to identify surface markers present on TA-EVs in a small cohort of preterm infants (n=27). TA-EVs in their cohort had elevated expression of CD326 and CD133, suggesting epithelial origin. Comparing the results by stage of lung development at birth, they found that CD24+ EVs were higher in those born in the late canalicular stage (22.1-26.6 weeks) compared to the saccular stage (27.0 to 34.6 weeks). Further, CD24+ and CD14+ EVs were higher in infants who developed BPD compared to those who did not. CD24 inhibits the NF-κB pathway, leading the authors to speculate that insufficient NF-κB caused by increased CD24 may result in reduced alveologenesis (83). CD14 is a marker of macrophages, and increased CD14+ EVs may therefore reflect increased inflammation in the lungs of infants who will go on to develop BPD. This study provided convincing evidence of the cellular origin of TA-EVs in preterm infants, however the importance of CD24 and CD14 in the development of BPD was not further explored.

While Wang *et al.* did not directly study TA-EVs, they isolated macrophages from the TA of preterm infants, cultured them, and then analyzed their EVs (84). They showed that these macrophage EVs contain miR-23a-3p, previously linked to vascularization and endothelial permeability (85,86). In this study, EV-encapsulated miR-23a-3p disrupted maintenance of the endothelial progenitor cell (EPC) pool and inhibited the endothelial function of the progeny of these EPCs. Silencing miR-23a-3p in a mouse model of BPD resulted in improved capillary density and alveolarization compared to untreated mice exposed to hyperoxia, demonstrating the pathological role of this exosomal miRNA in BPD.

Collectively, these five studies demonstrate the potential of TA-EVs to better understand the pathogenesis of BPD, especially the cellular responses of each lung cell type to factors associated with development of the condition.

Beyond TA, the role of EVs in blood of premature infants has been explored in BPD, with EV miRNAs receiving particular attention. Go *et al.* studied serum EVs, and found miR-21 to be significantly upregulated on day of life (DOL) 28 in premature infants who developed BPD compared to those who did not (87). However, as pointed out by Jenike & Halushka (88), miR-21 is a relatively ubiquitous miRNA, and its upregulation is also linked to IPF and pneumonia (89,90), which does not support the claim that it is a specific BPD biomarker. Zhong and colleagues compared umbilical cord blood (UCB) EVs of patients who developed BPD or not at DOL 0. They found that EV miR-103-3p and miR-185-5p expression was decreased in BPD patients. In vitro overexpression of these miRNA improved endothelial cell proliferation, suggesting involvement in BPD pathogenesis (91). Wang *et al*. compared circRNA, lncNRA and mRNA of EVs from UCB of premature infants with and without BPD (46). They showed that hsa_circ_0086913 and MAGI2-AS3 were upregulated, while hsa_circ_0007372, hsa_circ_0065188, BASP1-AS1 and SLC2A2-AS1 were downregulated in BPD. Although most of these RNAs have not previously been studied, there is some evidence for the involvement of MAGI2-AS3 in pathways related to BPD such as oxidative stress and senescence (92). These differentially expressed RNAs were associated with the mammalian target of rapamycin (mTOR) signalling pathway and extracellular matrix (ECM)-receptor interaction pathways. The implication of such RNAs in the pathophysiology of BPD was not further explored in this study. These studies collectively show that delivery of miRNA and other RNA by EVs likely contributes to the pathogenesis of the disease. However, the multifactorial nature of BPD limits the diagnostic applicability of this finding, as it is unlikely a single miRNA is responsible for the condition.

EVs have also been studied for their functional aspects in BPD. EVs from premature infants have been shown to be able to induce lung injury when given to healthy animals, suggesting a role in the

pathogenesis of BPD. Zhong *et al.* isolated EVs from UCB of preterm infants who developed BPD (93). These EVs were injected into mice exposed to hyperoxia, and it was shown that addition of the BPD-EVs worsened histological lung injury scores, increased collagen deposition, and decreased VEGFA and CD31 staining (indicating reduced angiogenesis) compared to mice only exposed to hyperoxia. Furthermore, BPD-EVs had a chronic effect on the lungs, with alveolar simplification, fibrosis and decreased VEGFA and CD31 staining persisting after a month in normoxia (post-natal day 42, P42). Analysis of gene expression in lung tissue of these mice showed that, compared to hyperoxia exposure alone, mice who received BPD-EVs had differential expression of genes related to angiogenesis and vascular remodelling. Therefore, it appears that UCB derived EVs from BPD patients are indeed involved in the pathogenesis of the condition.

Starke *et al.* collected plasma from premature infants who were receiving fraction of inspired oxygen (FiO_2) < 30 or FiO_2 > 30 (94). EVs isolated from the plasma of these infants were given by retro orbital sinus injection to newborn mice at P3 to assess the effect of the EVs on both the lung and brain. Lung histology demonstrated increased infiltration of macrophages, increased alveolar simplification and reduced vascular density, demonstrating that circulating EVs from patients on >30 FiO_2 worsened characteristics of lung injury. It is important to note that the patients receiving >30 FiO_2 were born earlier and had lower birth weights than those receiving <30 FiO_2. This means higher FiO2 is not necessarily responsible for the increased pathogenicity of the EVs, as these patients may simply have been sicker, requiring increased FiO_2. Nevertheless, these results contribute to the understanding of the biological function of EVs from premature infants.

Conversely, proteomics of EVs in BPD are understudied. At the time of writing, no studies have used untargeted proteomics approaches to evaluate proteins present in EVs isolated from biofluids of premature infants. Rather, studies have generally looked for evidence of specific proteins within EVs. For example, Ali *et al*. demonstrated that gasdermin D, involved in inflammasome-mediated cell death, is secreted in EVs by AT2 cells in the rat hyperoxia BPD model (95). Activation of the inflammasome

cascade has been previously implicated in the pathophysiology of BPD, suggesting that EVs may play a role in this process (96). The same group looked for evidence of apoptosis associated speck-like protein containing a caspase recruitment domain (ASC), which is necessary for inflammasome assembly, in circulating EVs and found higher expression in infants receiving high FiO_2 (94). Olave *et al*. found that fibroblast growth factor 2 (FGF2) was shown to be elevated in TA of one day old infants who developed BPD. They then showed that FGF2 released in EVs of bronchial epithelial cells increased following hyperoxia exposure and may have angiogenic effects (97). They speculate that FGF2, a growth factor involved both in lung development and disease, is released from injured epithelial cells to stimulate capillary growth. While these studies provide important knowledge of specific EV proteins that may have pathogenic roles in BPD, they also highlight the need to determine the protein cargo of EVs in lung disease more generally. As EVs are known to mediate cellular responses by protein transfer, among other methods, the lack of studies examining the proteome of EVs in premature infants represents a significant gap in the knowledge. Knowledge of the proteome of EVs from specific biofluids, such as tracheal aspirate, is essential to move towards more targeted approaches to studying EVs, as well as for formulating hypotheses on the role of EVs in neonatal diseases and physiology.

1.3.4 Flow cytometric approaches to studying EVs

Flow cytometric approaches for studying EVs have gained considerable attention in recent years. Through measurement of light scatter and fluorescence, flow cytometers are capable of simultaneously characterizing the size and proteins of single particles in a high-throughput manner, which, contrary to bulk analysis methods, provides information on the heterogeneity of EVs from a sample.

Evaluation of EVs by flow cytometry, hereafter referred to as nanoflow cytometry (nFC), presents unique challenges compared to cellular flow cytometry. Primarily due to the small size of EVs, there are particular aspects of flow cytometric protocols that must be considered to obtain meaningful and biologically relevant results. For example, as flow cytometers are designed for single-cell analysis, the sample core stream diameter is large enough to accommodate several EVs at once, which can lead to an

erroneous reading known as coincidence, or the swarm effect (98). To address this specific issue, EVs should be detected at low flow rates to reduce the sample flow diameter as much as possible, and serial dilutions of the EVs should be performed to ensure linear detection and absence of swarm (99). Additionally, the aggregation of fluorescent reagents, like antibodies used to phenotype EVs, can produce signals overlapping with the expected size and fluorescence of true EVs, therefore creating false positives. This can be mitigated by the use of buffer and reagent controls, in which the reagent is run in buffer to determine if it produces signals by itself (100).

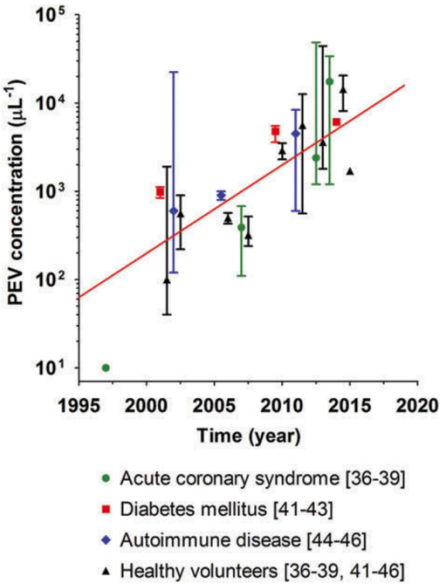

Figure 4. Platelet EV concentratons are increasing over time due to improvements in EV detection. Reproduced from (102).

In addition to the technical challenges posed by nFC, data analysis requires particular considerations. As flow cytometers produce data in arbitrary units, it is not possible to compare data across different instruments or institutions without calibration of both light scatter and fluorescence into standard units. Furthermore, as no flow cytometers currently have the ability to detect all EVs in a population, reporting the concentration over a specified range in standard units, rather than the population percentage, is paramount for comparability. These pitfalls, combined with a lack of clear reporting of instrument settings and steps taken for sample preparation, staining, acquisition, and data analysis, lead to the inability to reproduce published data.

These examples highlight the unique challenges associated with nFC. There exist several resources to produce high quality flow cytometric data when studying EVs, including the MiFlowCyt-EV reporting framework (101), which is endorsed by several international societies including the International Society for Extracellular Vesicles (ISEV), International Society for Advancement of Cytometry (ISAC), and International Society on Thrombosis and Haemostasis (ISTH). However, there

continue to be published reports that do not use appropriate controls, provide adequate proof of single vesicle detection, or report their protocols. The consequence of this is a lack of reproducibility in the field, an inability to compare results from different institutes, and inaccuracies in the biological interpretation of the data. A striking example of the impact of these consequences on biological interpretations was highlighted by Gąsecka *et al.*: over a ten year period, concentrations of platelet extracellular vesicles appeared to increase – a phenomenon due to improvement in detection strategies rather than actual biological changes (102).

1.3.4.1 Nanoflow cytometry for the study of lung disease

nFC has not been used to study EVs in the context of BPD but has been used for ARDS and COPD. In particular, EVs from leukocytes and endothelial cells appear to have potential as both biomarkers and in understanding disease pathogenesis. Bazzan and colleagues compared EVs in BALF of smokers with and without COPD. CD14+ EVs were positively correlated with pack-years of smoking, and inversely correlated with lung function in smokers with COPD (72). It is important to note that this study did not report the instrument settings for acquisition, nor did they provide adequate proof of single vesicle detection through the use of controls.

At the same time, Soni and colleagues found that increasing neutrophil EVs from BALF correlated with worse COPD severity and mortality (71). They also confirmed the presence of leukocyte, monocyte, alveolar macrophage, epithelial and platelet derived EVs in BALF. Several appropriate controls were used, including sample alone, detergent, and isotype controls. The gating strategies were also shown. A detailed protocol is available, which is beneficial for reproducibility, although instrument settings were not included. This study also measured CD14+ EVs in BALF, though they were not correlated with either pack-years of smoking, or with declining lung function, highlighting the discrepancies between studies that may arise due to the variations in pre-analytical variables, technical settings, and data analysis methods.

A very small study (n=3) looked at BALF EVs in patients with ARDS due to trauma and/or burn (103). CD44 and CD274 were strongly expressed on these EVs, and staining of CD11b, CD31, and CD16 were higher than CD9, CD63 and CD81. As CD44 contributes to injury response through monocyte proliferation and phagocytosis, this finding is interesting although requires further investigation. Some details on the staining protocol were available, and positive and negative EV controls were used. Instrument settings were not reported, and there was a lack of appropriate controls to prove the presence of single vesicle events.

These three studies provide crucial preliminary information on EVs in BALF but also highlight pitfalls of nFC. First, all were published following the availability of the MiFlowCyt-EV framework, which concisely summarizes some best-practices for nFC. The studies on which the framework is based were also available prior to the publication of these 3 studies. Yet, none used the reporting guidelines. Second, controls outlined in MiFlowCyt-EV and previously published research, including serial dilution controls and reagent and buffer controls, were not used, and it is therefore difficult to confirm if these papers are truly reporting on EVs. Lastly, none of the studies presented calibrated the arbitrary units of the cytometer into standard units, making comparison between different studies difficult. In order to produce data that has biological significance and can be reproduced, it is paramount to consider frameworks and reporting guidelines such as MiFlowCyt-EV.

2. Rationale, hypothesis and objectives

2.1 Rationale

BPD is the most common complication of prematurity and lacks effective treatment. The therapeutic potential of MSCs for the prevention and treatment of BPD has been extensively demonstrated and is currently being tested in early phase clinical trials. The mechanisms by which MSCs interact with cells of the premature lung remain incompletely understood. Here, we propose leveraging EVs, potent candidate biomarkers involved in cellular communication, to elucidate cross-talk between MSCs and resident cells of the premature lung, using a robust nFC approach. EVs have been shown to be sensitive biomarkers that reflect the state of their cell of origin, providing a surrogate for biopsy of the human lung.

2.2 Hypothesis

Given the summarized background on BPD, MSCs, and EVs, I expect that MSCs will attenuate inflammation in the lungs of premature infants by favouring anti-inflammatory cell phenotypes over pro-inflammatory ones. This will translate to increased EVs detected from anti-inflammatory cells. Furthermore, the attenuated inflammation will allow for proliferation of endothelial and epithelial cell populations that are typically ablated in BPD, which will cause increased detection of EVs from these cell populations.

2.3 Aims

The main objective of this project is to characterize EVs isolated from tracheal aspirates of infants enrolled in HULC-1, before and after they received MSCs. As a comparison group, we will also carry out all experiments on TA-EVs from HULC-Obs, which were taken at two timepoints, but infants were not treated with MSCs.

The aims of this project are therefore to:

1. Isolate EVs from tracheal aspirate using ultracentrifugation and characterize them with nanoparticle tracking analysis, protein measurements, and transmission electron microscopy
2. Identify the cellular origins of EVs isolated from tracheal aspirates using an antibody bead capture array for bulk analysis
3. Define changes in protein surface marker and cargo of EVs before and after treatment with MSCs, using single particle nanoflow cytometry and proteomics

3. Materials and methods

3.1 Institutional approvals

HULC-Obs was approved by Ottawa Health Science Network Research Ethics Board (OHSN-REB) under Protocol ID# 20190628-01K.

HULC-1 was approved by OHSN-REB under Protocol ID# 20220087-01K.

3.2 HULC-Obs

HULC-Obs was a prospective single-centre observational cohort study with the objective of assessing the feasibility of an interventional trial protocol prior to undertaking the actual trial. This was a novel approach to avoid failure of the clinical trial due to factors like patient and health care worker willingness to participate and also serves as a prospective cohort of control patients to the interventional cohort. Patients were included if they were admitted to the Ottawa Hospital General Campus Neonatal Intensive Care Unit (NICU), were born at less than 28 weeks' gestation, were between 7 and 21 days old and intubated on mechanical ventilation, and had parent or surrogate informed consent.

A total of 12 patients were enrolled in HULC-Obs. Serum and TA sample collection occurred at enrolment, and again 3-4 days later.

3.3 HULC-1

HULC-1 (NCT04255147) was a Phase I, multicenter, open-label, dose escalation study to evaluate the safety and feasibility of intravenous UC-MSCs for premature infants at high risk of developing BPD. Patients were included if they were admitted to the Ottawa Hospital General Campus NICU or Sunnybrook Health Sciences Center NICU, were born at less than 28 weeks' gestation, were between 7 and 28 days old and intubated on mechanical ventilation with $FiO2 \geq 30$, and had parent or surrogate informed consent. Three escalating dose panels were tested: 1.0×10^6 cells/kg, 3.0×10^6 cells/kg, and 10×10^6 cells/kg. Patients were enrolled in the lowest panel, and in the absence of adverse events, enrolment in the higher panels would begin.

A total of 9 patients were enrolled in HULC-1. Serum, TA and urine collection occurred at enrolment (before UC-MSC infusion), and again 3-4 days after UC-MSC infusion.

3.4 TA preparation and TA-EV Isolation

TA were collected by flushing approximately 1 mL of saline from the suction catheter and collected in a specimen trap. The sample was then placed in a cooler containing an ice pack for transport to the lab. TA was centrifuged 1,500 x g for 10 minutes at 4°C, and the supernatant (referred to as "cleared TA") was transferred to a cryovial for storage at -80°C. Cleared TA were further prepared once all study samples had been received by the lab.

Cleared TA were transferred to ultracentrifugation tubes and ultracentrifuged 100,000 x g for 90 minutes at 4°C using an Optima Max Ultracentrifuge (Beckman Coulter) with a TLA 100.3 rotor (Beckman Coulter). The supernatant was removed and stored. The pellet (or, in absence of a visible pellet, a small volume of supernatant) was resuspended in 100 µL of 0.1 µM filtered PBS (hereafter referred to as filtered PBS) and stored in five 20 µL aliquots. One aliquot was immediately used for nanoparticle tracking analysis (NTA), whereas the other four were immediately stored at -80°C.

3.5 Nanoparticle tracking analysis (NTA)

TA-EVs were measured on a ZetaView PMX110 (Particle Metrix, Meerbusch, Germany) calibrated with polystyrene beads and analyzed using the ZetaView software (version 8.04.02). EVs were serially diluted with filtered PBS until the concentration was in the working range of the instrument. EVs were measured at 11 camera positions. Raw data were adjusted to account for the dilution of each individual sample and imported into GraphPad Prism (version 10.3.1) for analysis.

3.6 Protein concentration

Protein concentration was measured using the micro bicinchoninic acid assay (BCA; Pierce Biotechnology #23235) in triplicate according to the manufacturer's instructions ("Microplate Procedure"). Briefly, 2 µL EVs were lysed in 48 µL RIPA buffer (ThermoFisher Scientific, #89900) with

1% protease inhibitor (Sigma-Aldrich #P8340) and incubated on ice for 30 minutes after mixing. The 50 µL EV lysate was diluted with 450 µL filtered PBS to ensure a 1:10 dilution of RIPA buffer. After addition of the working reagent, plates were incubated at 37°C for 2 hours. Absorbance was measured at 562 nm on a BioTek Synergy HT with Gen5 software. Raw data was imported into GraphPad Prism, where the standard curve equation was determined using a best-fit polynomial equation. Sample protein concentration was then interpolated using this equation.

3.8 Transmission electron microscopy (TEM)

TEM was carried out at the Nanoscale Biomedical Imaging Facility at SickKids (Toronto, ON, Canada). Briefly, 2 µL from each EV sample were pooled into 4 groups (HULC-Pre, HULC-Post, Obs-Pre, Obs-Post) to obtain a mean particle concentration of 1.38E+11 particles/mL. Each pooled sample was combined with an equal volume of 4% paraformaldehyde (PFA) for fixation and shipped on dry ice to the facility. EVs were stained with 2% uranyl acetate and imaged with Hitachi HT7800 TEM and EMSIS Xarosa complementary metal oxide semiconductor (CMOS) camera.

3.9 Mass spectrometry

To achieve three replicates of 10 µg of protein each, samples were randomized and pooled to achieve equal amount of protein from each. To a pooled sample volume of approximately 30 µL, approximately 15 µL of RIPA and 1% protease inhibitor was added. Samples were allowed to incubate on ice for 30 minutes to achieve lysis. Samples were then snap frozen in liquid nitrogen.

Proteomics analysis was performed at the Ottawa Hospital Research Institute Proteomics Core Facility (Ottawa, Canada). An aliquot of EV lysate containing 10µg of protein was diluted to 50µL with 50mM ammonium bicarbonate (ABC). The proteins were denatured by heating the samples at 95°C for five minutes and then dithiothreitol (DTT) was added to a concentration of 5mM followed by a 30min incubation at 56°C. The samples were allowed to cool and the reduced disulfide bonds were alkylated with the addition of iodoacetamide to a concentration of 25mM followed by an incubation in the dark for

30 minutes. 200µg of washed SP3 magnetic beads (50:50 mix of hydrophilic and hydrophobic beads, Cytiva) were added to the protein lysate and ethanol was added to a concentration of 50%. The proteins were bound to the beads during a 15-minute incubation. The beads were washed three times with 80% ethanol and then air-dried. 50µL of digestion buffer containing 50mM ABC, 5% acetonitrile, 1mM CaCl2, and 500ng of sequencing-grade trypsin-LysC protease (Promega) was added to each sample and the proteins were digested on-bead overnight at 37°C.

The supernatant was transferred to a fresh tube and the beads were washed once again with 50mM ABC. The supernatants were combined and dried in a speed-vac. The peptides were resuspended in 0.1% trifluoroacetic acid (TFA) and desalted with C18 Stagetips prepared in-house. The desalted peptides were dried and resuspended in 0.1% formic acid. The peptide concentration of each sample was determined by Nanodrop spectrometer (λ=280nm) and the volume-equivalent of 1ug was injected into the LC-MS. The peptides were separated using a Dionex Ultimate 3000 RLSC nano HPLC along a ninety-minute reversed-phase gradient with a 2cm PEPMAP 100 C18 Precolumn and a 50cm Acclaim PEPMAP C18 analytical column (Thermofisher Scientific). The HPLC was coupled by electrospray ionization to an Orbitrap Fusion Lumos tribrid mass spectrometer (Thermofisher Scientific) operating in data-dependent acquisition mode. MS1 data was acquired with the Orbitrap detector at a resolution of 240,000 with a standard AGC target of 100% and an automatically determined maximum fill time. The scanning mass range was 350-1600 m/z and the RF lens voltage was set to 60%. MS2 data was acquired in the linear ion trap for the 25 most intense ions with an AGC target of 100% and a quadrupole isolation width of 1.6 m/z. Precursors selection for fragmentation was based on an enabled dynamic exclusion of 60 s with a normalized HCD fragmentation energy of 35%.

The acquired raw data was searched using Fragpipe software (version 21.1) (104) and matched against a UniProt human protein sequence database including canonical and isoform-reviewed sequences (retrieved August 2024). The database included of common contaminants. Two missed cleavages were permitted along with the variable oxidation of methionine, the variable acetylation of the protein N

terminus, and the fixed carbamidomethylation of cysteine residues. Relative label-free protein quantitation was calculated using MS1-level peak integration, the application of the MaxLFQ algorithm, and enabling the matching-between-runs feature enabling a 3 min retention time matching window. False discovery rate (FDR) was set to 1% for peptide spectral matches using a target-decoy strategy. The results were exported to Scaffold (Proteome Software, USA) for further validation and viewing, including filtering for proteins identified by a minimum of two peptides.

For analysis, only proteins for which more than two peptides had been detected were kept. Contaminant, decoy, reverse, and non-human proteins were removed, along with proteins not detected in all replicates. Remaining proteins were sorted by abundance using the log2 of the MaxQuant label-free quantification (MaxLFQ) method to determine the top 20 most abundant proteins.

3.10 Antibody capture bead assay

Bead-based flow cytometry was carried out using the MACSPlex IO EV Kit (Miltenyi Biotec #130-108-813). Following titration to determine the optimal number of particles necessary for adequate signal detection, we calculated the volume necessary to input 1E+8 particles from each sample (HULC-Obs n=20; HULC-1 n=16). We followed the "Overnight protocol for the assay using 1.5mL tubes" protocol provided by the manufacturer. Briefly, the calculated volume of sample was diluted up to 120 µL with MACSPlex buffer. 15 µL of MACSPlex EV Capture Beads were added to each tube and incubated overnight. Excess beads were removed by centrifugation, and 5 µL each of allophycocyanin (APC)-conjugated CD9, CD63 and CD81 antibodies were added and incubated for 1 hour. Following two wash steps, beads were resuspended and transferred to flow tubes for analysis on the Cytek Aurora. Beads were gated per the manufacturer's protocol (**Figure 7B-C**). APC fluorescence intensity was calibrated from arbitrary units (a.u.) to molecules of equivalent soluble fluorophore (MESF) using Quantum MESF beads (Bangs Labs #823). Gain was adjusted as follows: forward scatter (FSC) 100, side scatter 100, and side scatter from the blue laser, 100. All detectors were adjusted to -75%, except the Red detector (R1-A) which was adjusted to +20% to better resolve the APC signal.

For data analysis, the approach of Welsh *et al.* was used (105). Briefly, data was imported into GraphPad Prism. Data was scaled logarithmically, as opposed to linearly, since it is superior for separation of high, medium and dim signals (105). Data was normalized by calculating the fold change of the median fluorescence intensity (MFI) of the positive bead divided by the MFI of the negative bead, referred to hereafter as the normalized staining intensity. This was chosen over blank subtraction to avoid the creation of negative numbers, which would interfere with logarithmic transformation of data.

3.11 Nanoflow cytometry (nFC)

EVs were stained with a combination of carboxyfluorescein succinimidyl ester (CFSE) and CellMask Green (CMG) to determine the concentration of total EVs. 8-point titrations of all reagents were conducted on a pooled TA-EV sample to experimentally determine the optimal concentration. A solution of 1:500 CMG and 20 μM CFSE was added to EVs (volume double that of the staining solution) and incubated for 25 minutes at 37°C. This was followed by a two hour incubation at 4°C in the dark with phycoerythrin (PE) conjugated antibodies against CD31 (endothelial derived), CD45 (immune derived), CD326 (epithelial derived), CD86 (M1 macrophage derived) and CD206 (M2 macrophage derived) to determine EV cellular origin (see **Table 2** for reagents). We performed unstained sample, serial dilution, buffer, buffer and reagent, single stain, detergent and isotype controls as suggested by the MiFlowCyt-EV framework to demonstrate presence of single vesicles (101).

Table 2. Reagents used for nFC.

Reagent	Cell target	Source	Catalogue number	Final staining concentration
CFSE	Intracellular proteins	Invitrogen	C34554	5 μM
Cell Mask Green	Membrane	Invitrogen	C37608	1:2000
CD31	Endothelial cells	BD Biosciences	555446	1 μg/mL
CD45	Leukocytes	Biolegend	304008	0.25 μg/mL
CD326	Epithelial cells	Biolegend	324206	1 μg/mL
CD86	M1 macrophages	Biolegend	305405	0.5 μg/mL
CD206	M2 macrophages	Biolegend	321105	0.5 μg/mL

For acquisition, samples were diluted with filtered PBS and events were recorded for one minute at a flow rate of 10 µL/min. Violet side scatter (V-SSC), FITC, and PE intensity in arbitrary units (a.u.) were calibrated in FCM_{PASS} (106) to EV Diameter in nanometers, Alexa Fluor 488 equivalent reference fluorophore (AF488 ERF), and PE MESF respectively.

For analysis, we considered EVs to be events between 110-1000 nm, staining positive for the dyes and antibody, and that were sensitive to detergent lysis (1% Triton X-100, Sigma-Aldrich #T9284). The median lower limit of the fluorescence ranges examined were 1100 AF488 ERF (IQR 1000 – 1200) and 70 PE MESF (IQR 65 – 76.25). Upper limits were 1.6E+6 AF488 ERF and 1.6E+5 PE MESF. The concentration of EVs was calculated by multiplying EVs by the dilution factors used for acquisition and staining. Gating and calculation of concentrations were done in a blinded fashion. We then compared EV measurements from the same patients before and after they received MSCs using the Wilcoxon matched-pairs signed rank test.

Further details of the experiment are reported according to the MiFlowCyt-EV framework in **Appendices A** and **B**.

3.12 Statistical analysis

All statistical analysis was performed using GraphPad Prism (version 10.3.1). Categorical values were compared using Fisher's exact test. Normality was assessed using the Shapiro-Wilks test. Normally distributed variables were compared using either the paired or unpaired t-test, and presented as mean and standard deviation (SD). Variables that were not normally distributed were compared using either the Wilcoxon signed-pairs matched-ranks test or the Mann-Whitney test, and presented by median and interquartile range (IQR).

4. Results

4.1 Characteristics of study cohorts

Nine patients were enrolled in HULC-1, and twelve were enrolled in HULC-Obs. Maternal and patient demographics are summarized in **Table 3**. The average gestational age of the patients was 24^{+3} (range of $23^{+1} – 26^{+4)}$ in HULC-1, and 25^{+0} (range of $23^{+6} – 27^{+1}$) in HULC-Obs, demonstrating that all study participants were extremely preterm.

In HULC-Obs, TA samples were collected from all 12 patients at one timepoint. “Post” samples were collected 3 to 4 days after the first collection point, but no cell therapy was administered to these patients. In this cohort, two Post samples were not collected: one due to patient death, and the other for unknown reasons. Two TA samples were further excluded due to lack of detection of particles or lack of protein detection. In HULC-1, TA were collected from all nine patients prior to receiving MSCs. Post-MSC samples were collected 3 to 4 days after patients were treated. One sample was not collected post-MSC as the patient had already been extubated, so it was not possible to collect TA. An additional TA sample was excluded due to lack of particle detection by NTA. Although protein was detected for this sample, the concentration was quite low, so it was determined that the sample was likely of poor quality.

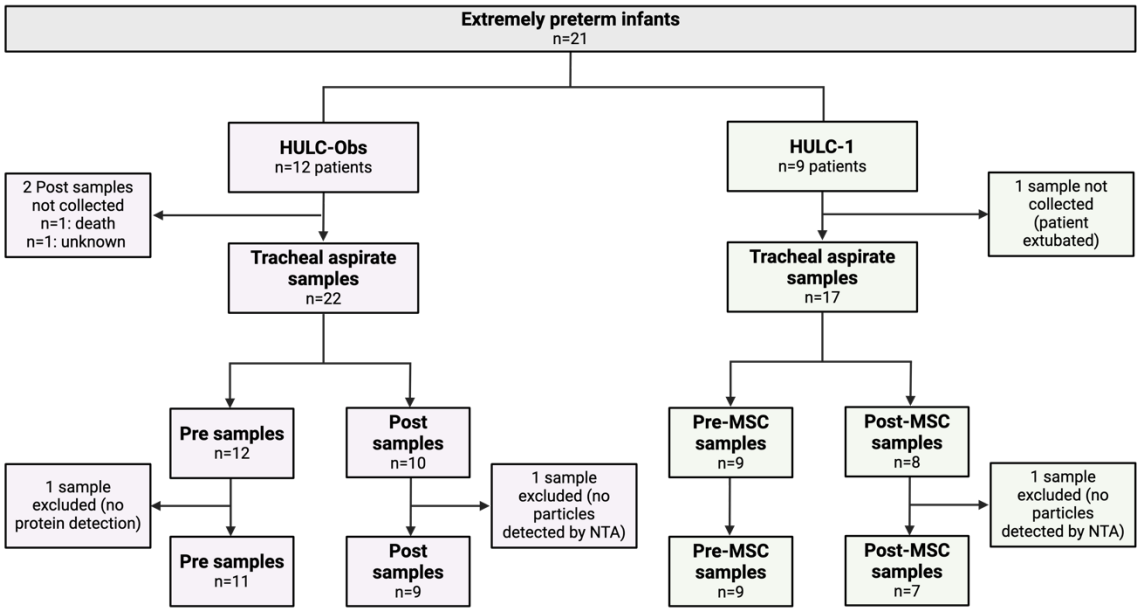

Figure 5. Flow diagram of TA samples obtained from infants enrolled in HULC-1 and HULC-Obs.

It is worth noting that sampling of infants in HULC-1 occurred at a significantly older age compared to HULC-Obs (Pre samples: unpaired t test, $P = 0.0005$. Post samples: unpaired t test, $P = 0.0019$).

Infants experienced a variety of complications associated with prematurity, as well as surgeries to correct some of these complications. They are summarized in **Table 4**. MSCs did not lead to any SAE in HULC-1.

Table 3. Demographics of patients enrolled in HULC-Obs and HULC-1.

	HULC-Obs n=12	HULC-1 n=9	
Maternal demographics (%)			
Type of delivery			
Vaginal	5 (41.7)	5 (55.6)	
C-section	7 (58.3)	4 (44.4)	
Antenatal gluco-corticoids			
none	2 (16.7)	2 (22.2)	
1 dose	0	0	
2 doses	10 (83.3)	6 (66.7)	
Unknown	0	1 (11.1)	
Preeclampsia	0	0	
Gestational diabetes	0	0	
Placental abruption	1 (8.3)	0	
Clinical chorioamnionitis	0	1 (11.1)	
PROM (>24 hours)	4 (33.3)	3 (33.3)	
IUGR	1 (8.3)	0	
Patient demographics			
Gestational age, (weeks^{+days}), mean (range)	25^{+0} (23^{+6} – 27^{+1})	24^{+3} (23^{+1} – 26^{+4})	
Birth weight, grams ,mean(SD)	675 (145.0)	647 (131.4)	
Sex (Female/Male)	7/5	4/5	
Age at MSC administration, mean (SD)	n/a	19.3 (6.1)	
Dexamethasone (%)	9 (75)	6 (66.7)	
Mechanical ventilation, Total days, mean (SD)	43.4 (32.8)	43.8 (14.3)	
Ventilation days since MSC administration, mean(SD)	n/a	24.9 (15.8)	
Total days NIPPV or CPAP, mean(SD)	49.1 (27.5)	n/a	
Total number of days on NIPPV/CPAP since MSC administration, mean(SD)	n/a	50.6 (17.7)	
Day of life first sample (mean+SD)	10.83 (3.2)	19.33 (6.1)	*
Day of life second sample (mean+SD)	14.4 (3.2)	23.13 (6.6)	*
Baseline Surgical Procedures	0	0	
Post Surgical Procedures(%)	2 (16.7)	4 (44.4)	
Sepsis (%)	7 (58.3)	6 (66.7)	
CLD at 36 weeks corrected age, N (%)	10 (83.3)	9 (100)	
Unknown	1 (8.3)	0	
Mild	2 (16.7)	2 (22.2)	
Moderate	5 (41.7)	2 (22.2)	
Severe	2 (16.7)	5 (55.5)	
CLD at 40 weeks corrected age, N (%)	7 (58.3)	7 (77.8)	
Unknown	2 (16.7)	0	
Mild	1 (8.3)	2 (22.2)	
Moderate	2 (16.7)	2 (22.2)	
Severe	2 (16.7)	3 (33.3)	
Discharged home on O2 (%)	3 (25)	7 (77.8)	
Death (%)	1 (8.3)	0	

PROM, premature rupture of membranes; IUGR, intrauterine growth restriction; MSC, mesenchymal stromal cell; NIPPV, non-invasive positive pressure ventilation; CPAP, continuous positive airway pressure; CLD, chronic lung disease (alternate name for BPD); O2, oxygen.

No significant differences were observed between cohorts (unpaired t-test for continuous data, $P > 0.05$; Fischer's exact test for categorical data, $P > 0.05$) unless indicated by *.

CLD was measured according to the definition of the Canadian Neonatal Network (3).

Table 4. Complications of prematurity experienced by enrolled infants at two timepoints.

	HULC-Obs n=12	HULC-1 n=9
Baseline complications of prematurity (%)		
Air leaks (pneumothorax)	2 (16.7)	1 (11.1)
Pulmonary interstitial emphysema (PIE)	1 (8.3)	1 (11.1)
Pulmonary hemorrhage (PH)	4 (33.3)	0
Necrotizing enterocolitis (NEC)	0	1 (11.1)
Patent ductus arteriosus (PDA)	10 (83.3)	4 (44.4)
Intraventricular hemorrhage	5 (41.7)	3 (33.3)
Grade I	1 (8.3)	1 (11.1)
Grade II	2 (16.7)	2 (22.2)
Grade III	1 (8.3)	0
Grade IV	1 (8.3)	0
Periventricular leukomalacia (PVL)	0	0
Intestinal perforation	0	0
Retinopathy of prematurity (ROP)	0	0
Post complications of prematurity (%)		
Air leaks (pneumothorax)	1 (8.3)	0
Pulmonary interstitial emphysema (PIE)	1 (8.3)	0
Pulmonary hemorrhage (PH)	1 (8.3)	0
Necrotizing enterocolitis (NEC)	1 (8.3)	1 (11.1)
Patent ductus arteriosus (PDA)	1 (8.3)	3 (33.3)
Intraventricular hemorrhage	3 (25)	2 (22.2)
Grade I	2 (16.7)	1 (11.1)
Grade II	1 (8.3)	1 (11.1)
Grade III	0	0
Grade IV	0	0
Periventricular leukomalacia (PVL)	1 (8.3)	1 (11.1)
Intestinal perforation	1 (8.3)	0
Retinopathy of prematurity (ROP)	1 (8.3)	2 (22.2)
Baseline surgery (%)	0	0
Post surgery (%)	2 (16.7)	5 (55.5)
Laparotomy	0	0
NEC surgery	0	0
Tracheostomy	0	1 (11.1)
Craniotomy/shunt insertion	0	0
PDA surgically ligated	1 (8.3)	2 (22.2)
Peritoneal drain	1 (8.3)	0
Other	0	2 (22.2)

Baseline: complication or surgery occurring prior to UC-MSC administration (HULC-1) or prior to enrolment (HULC-Obs)**; Post:** complication or surgery occurring after MSC administration (HULC-1) or after enrolment (HULC-Obs).
No significant differences were observed between cohorts (Fischer's exact test, $P > 0.05$).
PDA refers to medically treated PDA. ROP refers to severe ROP (stage 3 or greater) or treated ROP. NEC refers to severe NEC (stage 2 or greater).

4.2 Tracheal aspirate contains extracellular vesicles

EV size, concentration, protein concentration and morphology are basic measurements for characterization of an EV population. Beyond being critical for planning downstream experiments, they

provide evidence of the presence of EVs in a preparation. This is especially important when working with TA-EVs, which have not been extensively evaluated in the literature. We therefore conducted experiments to determine the concentration of particles and protein, performed TEM to evaluate the morphology of the particles, and used mass spectrometry to evaluate the presence of proteins commonly enriched in EVs (107).

4.2.1 Particle size and concentration does not change after MSC treatment

NTA was conducted on all TA-EV samples and demonstrated the presence of particles up to 1 μm in 21 out of 22 samples in HULC-Obs, and in 16 out of 17 samples in HULC-1. EV samples in which no particles were detected were excluded from further analysis as they were of poor quality. The size distribution of all included samples (n=36) is shown in **Figure 6B**. The median particle size in HULC-Obs (n=20) was 177.8 nm [IQR 165.9 – 221.0] and 173.6 nm [IQR 151.7 – 190.5] in HULC-1 (n=16, **Figure 6C**). The median concentration of particles was 1.02E+11 particles/mL [IQR: 3.83E+10 – 2.22E+11] in HULC-Obs, and 2.22E+11 particles/mL [IQR: 6.33E+10 – 2.78E+11] in HULC-1 (**Figure 6D**). No difference was noted between cohorts, nor between the pre- and post-samples of either cohort. Comparison of pre- and post-MSC measurements in HULC-1 are shown in **Figure 6F-G**.

4.2.2 Protein concentration is not altered after MSC treatment

Protein concentration of TA-EV samples was measured using the micro BCA assay. We excluded one sample from HULC-Obs in which no protein was detected. The median protein concentration was 590.3 [IQR 298.2 – 804.6] and 635.1 μg/mL [IQR 282.4 – 1075.0] in HULC-Obs and HULC-1, respectively (Figure **6E**). No difference was noted between cohorts, nor between the pre- and post-samples of either cohort. Comparison of pre- and post-MSC measurements in HULC-1 are shown in Figure **6H**.

4.2.3 Transmission electron microscopy reveals morphology of TA-EVs

Morphology of TA-EVs was assessed using transmission electron microscopy (TEM), which revealed the presence of EVs of various sizes. Morphology of EVs was similar across all groups (HULC-Obs Pre, HULC-Obs Post, HULC-1 Pre-MSCs, HULC-1 Post-MSCs) and images are displayed in **Figure 6I-L**.

These preliminary characterization experiments demonstrate the presence of particles up to 1 μm in TA. Particle size, concentration, and protein concentration did not vary between cohorts, suggesting that TA-EVs from both groups are comparable. Similarities between EV morphologies further confirmed this. While these measurements can provide evidence regarding the state of the cell of origin or disease pathology, we did not observe any differences following the treatment with MSCs in the HULC-1 cohort.

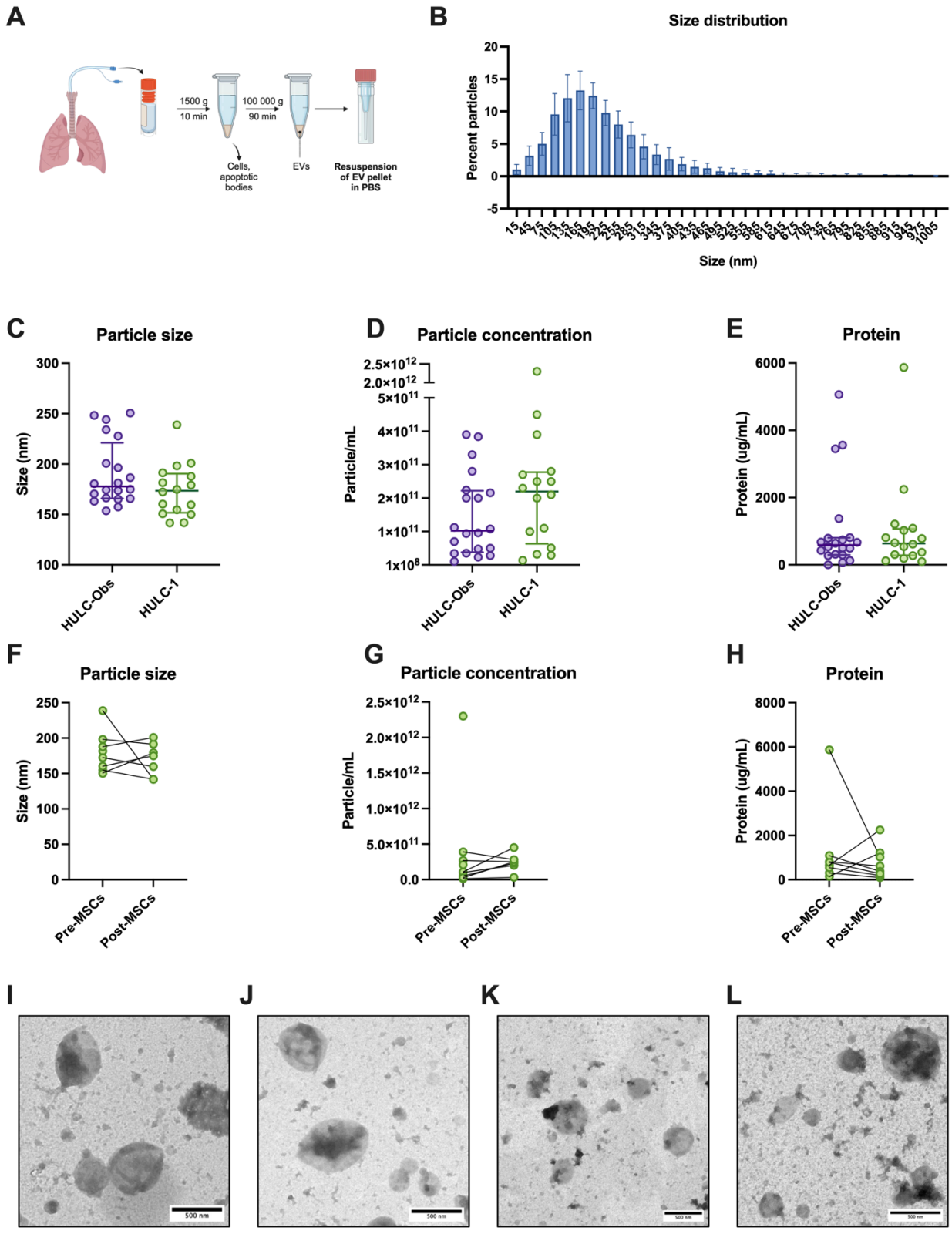

Figure 6. Characterization of TA-EVs. (**A**) Schematic overview of experimental design. (**B**) Size distribution of all TA-EVs (n=36). Bars show mean and standard deviation. (**C**) Particle size (nm) of samples from HULC-Obs (n=20) and HULC-1 (n=16). (**D**) Particle concentration (particle/mL) of samples from HULC-Obs (n=20) and HULC-1 (n=16). (**E**) Protein concentration of samples from HULC-Obs (n=20) and HULC-1 (n=16). Bars show median and interquartile range unless stated otherwise. Comparison of particle size (**F**), particle concentration (**G**), and protein concentration (**H**) measurements pre- and post-MSCs in HULC-1 cohort. TEM images of pooled EVs HULC-Obs Pre (**I**), HULC-Obs Post (**J**), HULC-1 Pre-MSCs (**K**) and HULC-1 Post-MSCs. Scale bar is 500 nm. *TA-EVs, tracheal aspirate extracellular vesicles; MSC, mesenchymal stromal cell; NTA, nanoparticle tracking analysis. TEM, transmission electron microscopy.*

4.3 TA-EVs originate from lung epithelium and immune cells

Identification of surface markers present on EVs provides information on their cell of origin. Antibody capture bead arrays are flow cytometric assays that allow for multiplexed evaluation of EV surface markers in a sample, while using small volumes of material. The MACSPlex EV Kit (Miltenyi) examines 37 different surface markers, providing information on the cellular origin of EVs in tracheal aspirate. This assay also allows us to verify that TA-EVs express common EV markers CD9, CD63, and CD81 at their surface.

The normalized staining intensity is presented in a heatmap in Figure **7D**. Normalized staining intensity of EV markers CD9, CD63 and CD81 beads in TA-EV samples was elevated compared to the blank control (CD9: 1.54, CD63: 1.57, CD81: 1.5) indicating enrichment of EVs in the sample (Figure **7E**). Other markers that were strongly detected included CD326, HLA-DRDPDQ, CD133, and CD24 (normalized staining intensity of 1.04, 1.17, 1.51 and 1.57, respectively; Figure **7F**). The presence of these markers strongly suggests that TA-EVs originate from lung epithelium and immune cell populations.

Markers present on TA-EVs were compared from the same patients before and after they received MSCs, however no significant differences were noted.

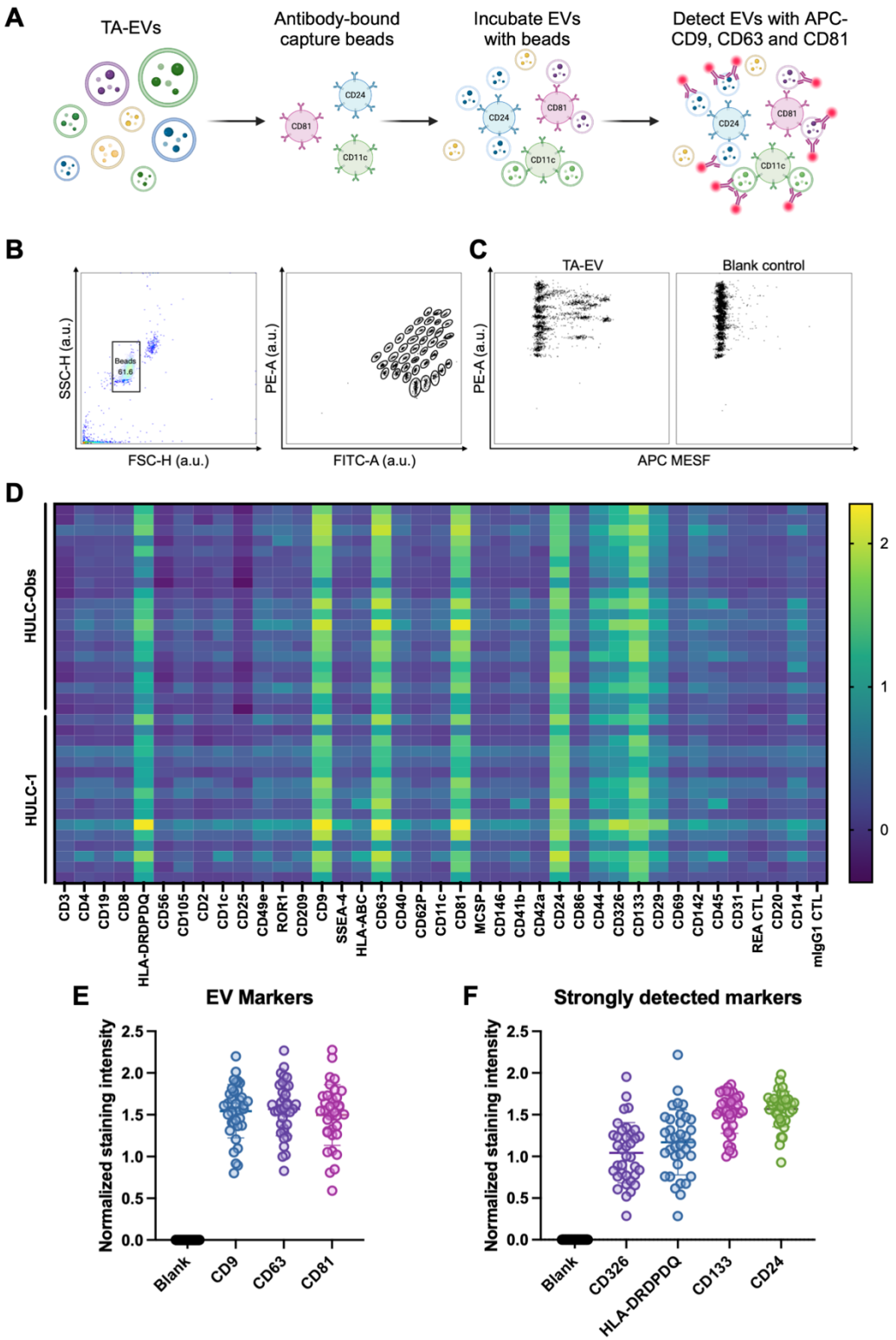

Figure 7. Multiplexed analysis of TA-EV surface markers. (**A**) Schematic overview of MACSPlex assay. (**B**) Gating strategy to identify the bead populations in the kit. (**C**) Representative dot plot demonstrating typical signal of a TA-EV sample and a blank control. (**D**) Heatmap showing normalized staining intensity of samples from HULC-Obs (n=20) and HULC-1 (n=16). Normalized staining intensity is defined as the log10 transformed APC MESF fold change from the blank. (**E**) Normalized staining intensity of EV markers CD9, CD63 and CD81. Bars show mean and standard deviation. (**F**) Normalized staining intensity of strongly detected surface markers. Bars show mean and standard deviation. *TA-EV, tracheal aspirate extracellular vesicle; SSC-H Side scatter height; FSC-H Forward scatter height; a.u. arbitrary units; PE phycoerythrin; FITC fluorescein isothiocyanate; APC allophycocyanin; MESF molecules equivalent soluble fluorophore.*

4.4 TA-EVs increase following MSC treatment

Characteristics of single EVs such as their surface markers and size can be measured by nFC. We can therefore use this technique to measure differences in surface markers of TA-EVs following administration of MSCs in premature infants, providing us with information about the cell of origin's response to the treatment. All concentrations presented here refer to EVs between 110-1000 nm in diameter, and within a lower limit of detection of 1100 AF488 ERF (IQR 1000 – 1200) and 70 PE MESF (IQR 65 – 76.25), and upper limits of 1.6E+6 AF488 ERF and 1.6E+5 PE MESF.

Total EVs measured after treatment with MSCs were elevated compared to pre-treatment samples in HULC-1 (n=7). Prior to receiving MSCs, the median total EV measurement was 4.6E+10 EVs/mL [IQR: 1.5E+10 – 1.2E+11], while 3-4 days after receiving MSCs, the median increased to 1.81E+11 EVs/mL [IQR: 7.6E+10 – 2.98E+11] ($P = 0.0156$, Figure **8B**-**C**). We did not observe the same increase in the HULC-Obs cohort (n=8, Pre: 2.2E+11 EVs/mL [IQR: 4.93E+10 – 5.28E+11], Post: 2.57E+11 EVs/mL [IQR: 2.3E+10 – 8.13E+11], $P > 0.05$), suggesting that the increase in EVs was not due to the maturation of the infants, but rather the treatment with MSCs (Figure **8D**-**E**). When looking at EVs positive for the surface markers tested, we saw no consistent trend across patients, and the Wilcoxon test did not demonstrate any significant difference after treatment with MSCs (Figure **8F**-**J**). Treatment with MSCs led to an increase in TA-EVs, however we did not identify consistent changes in EVs released from the specific cell types tested before and after the treatment.

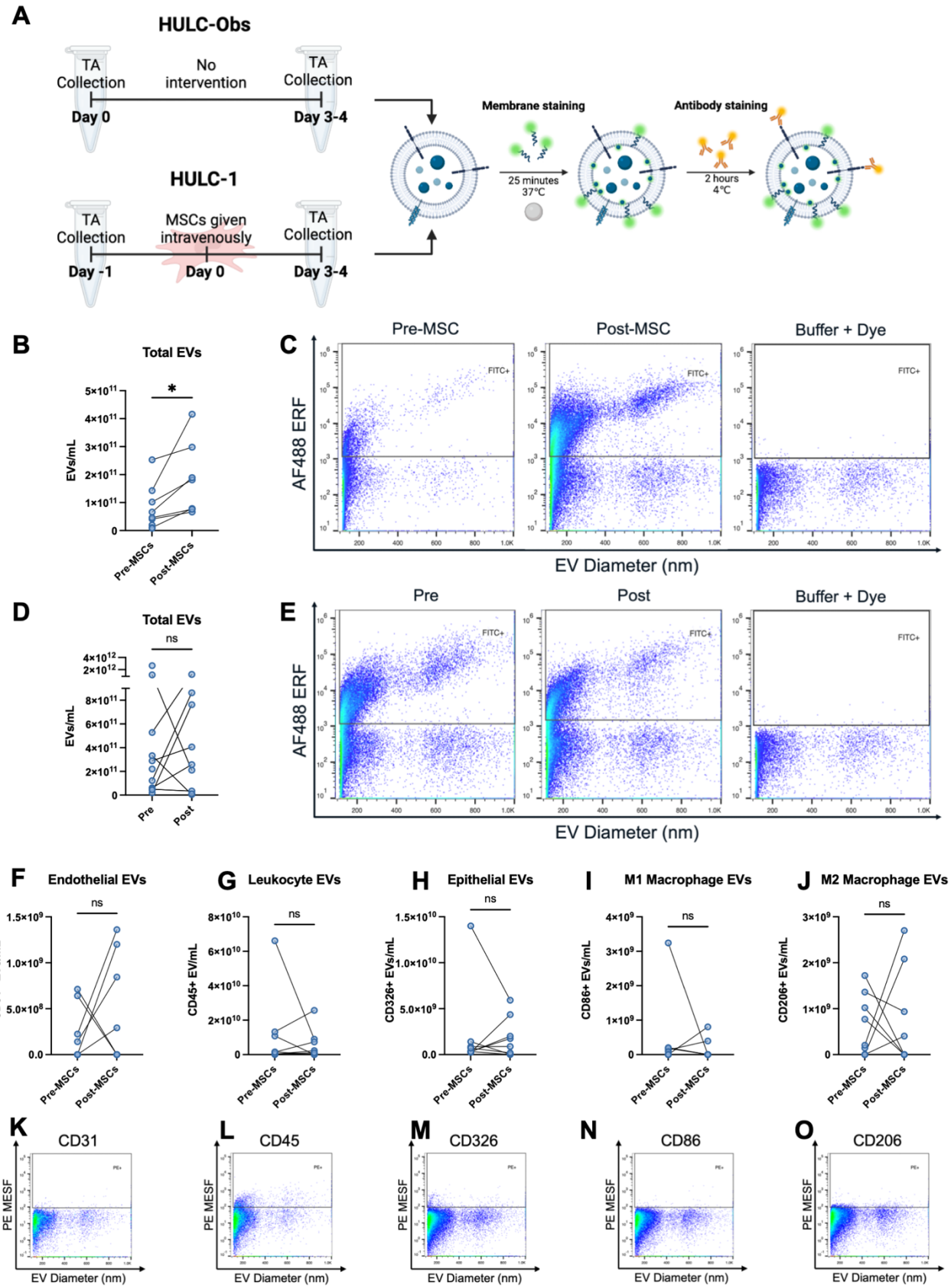

Figure 8. Nanoflow cytometric measurement of TA-EVs. (**A**) Schematic overview of experimental design. (**B**) Comparison of EVs/mL measured in HULC-1 before and after treatment with MSCs. Wilcoxon matched-pairs signed rank test, n=7, *P < 0.05. (**C**) Representative flow plots showing EVs from the same patient in HULC-1 before and after treatment with MSCs, as well as a buffer and dye control. (**D**) Comparison of EVs/mL measured in HULC-Obs at two timepoints, 3-4 days apart. Wilcoxon matched-pairs signed rank test, n=8, ns > 0.05. (**E**) Representative flow plots showing EVs from the same patient in HULC-Obs at two timepoints, 3-4 days apart, as well as a buffer and dye control. EVs originating from endothelial cells (**F**), leukocytes (**G**), epithelial cells (**H**), M1 macrophages (**I**), and M2 macrophages (**J**) were not different in HULC-1 before and after treatment with MSCs.

TA-EV, tracheal aspirate extracellular vesicles; MSC, mesenchymal stromal cell; AF488 ERF, Alexa Fluor 488 Equivalent Reference Fluorophore; PE MESF, phycoerythrin molecules of equivalent soluble reference fluorophore.

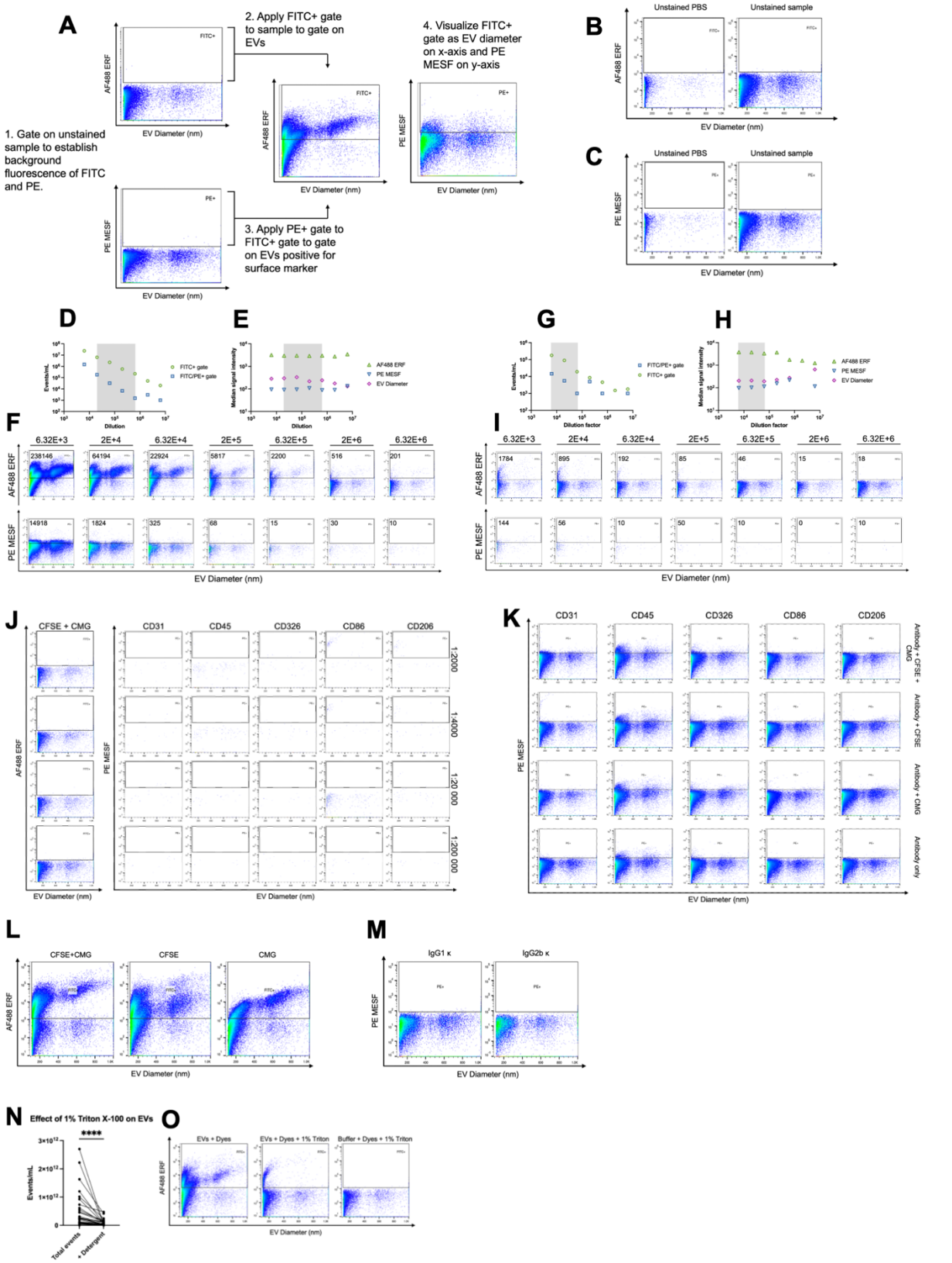

Figure 9. Nanoflow cytometric controls. (**A**) Gating strategy used to identify EVs and EV positivity for surface markers. (**B**) Unstained PBS and EV sample controls in the FITC channel. (**C**) Unstained PBS and EV sample controls in the PE channel. In a concentrated sample, events/mL in the FITC+ or FITC/PE+ gate, (**D**) and median signal intensity of AF488, PE and EV Diameter (nm) (**E**) are plotted against the dilution used for acquisition. Grey bar shows the linear region. (**F**) Flow plots of a serial dilution of a concentrated sample. Dilution is indicated above the plot, and the number of events detected is indicated in the gate. Top row shows AF488 staining, and bottom row shows PE staining. In a dilute sample, events/mL in the FITC+ or FITC/PE+ gate, (**G**) and median signal intensity of AF488, PE and EV Diameter (nm) (**H**) are plotted against the dilution used for acquisition. Grey bar shows the linear region.

Continued next page.

Figure 9 continued. (**I**) Flow plots of a serial dilution of a dilute sample. Dilution is indicated above the plot, and the number of events detected is indicated in the gate. Top row shows AF488 staining, and bottom row shows PE staining. (**J**) Buffer controls of membrane dyes and antibodies at various acquisition dilutions. (**K**) Fluorescence-minus-one controls for each antibody used in the study. (**L**) Fluorescence-minus-one controls for the membrane dyes used for EV staining. (**M**) Isotype controls IgG1k (for CD31, CD45, and CD206) and IgG2bk (for CD326 and CD86). (**N**) Comparison of total events before and after treatment with 1% Triton X-100. Wilcoxon matched-pairs signed rank test, n=39, ****P<0.0001. (**O**) Representative flow plots showing a sample of stained EVs, the same sample stained with 1%, and the dyes and Triton in buffer. *PE phycoerythrin; FITC fluorescein isothiocyanate; AF488 ERF, AlexaFluor 488 equivalent reference fluorophore; MESF molecules equivalent soluble fluorophore; CFSE carboxyfluorescein succinimidyl ester; CMG CellMask Green.*

4.4.1 Large CD31+ EVs increase following MSC treatment

During analysis, it was noted that on flow cytometry plots, TA-EVs tended to form two distinct populations: one between 110-400 nm, and the other between 400-1000 nm. Given that these two populations were observed consistently across all samples, we decided to perform the analysis from **Section 4.4** on each size population. When sizes were analyzed separately, neither the smaller nor the larger EVs in the HULC-1 cohort were significantly elevated, demonstrating that the increase in EVs is not dependent on a specific EV size. Interestingly, the size difference analysis did identify that EVs between 400-1000 nm and positive for CD31 were significantly elevated after treatment with MSCs. No significant differences were observed in the HULC-Obs cohort.

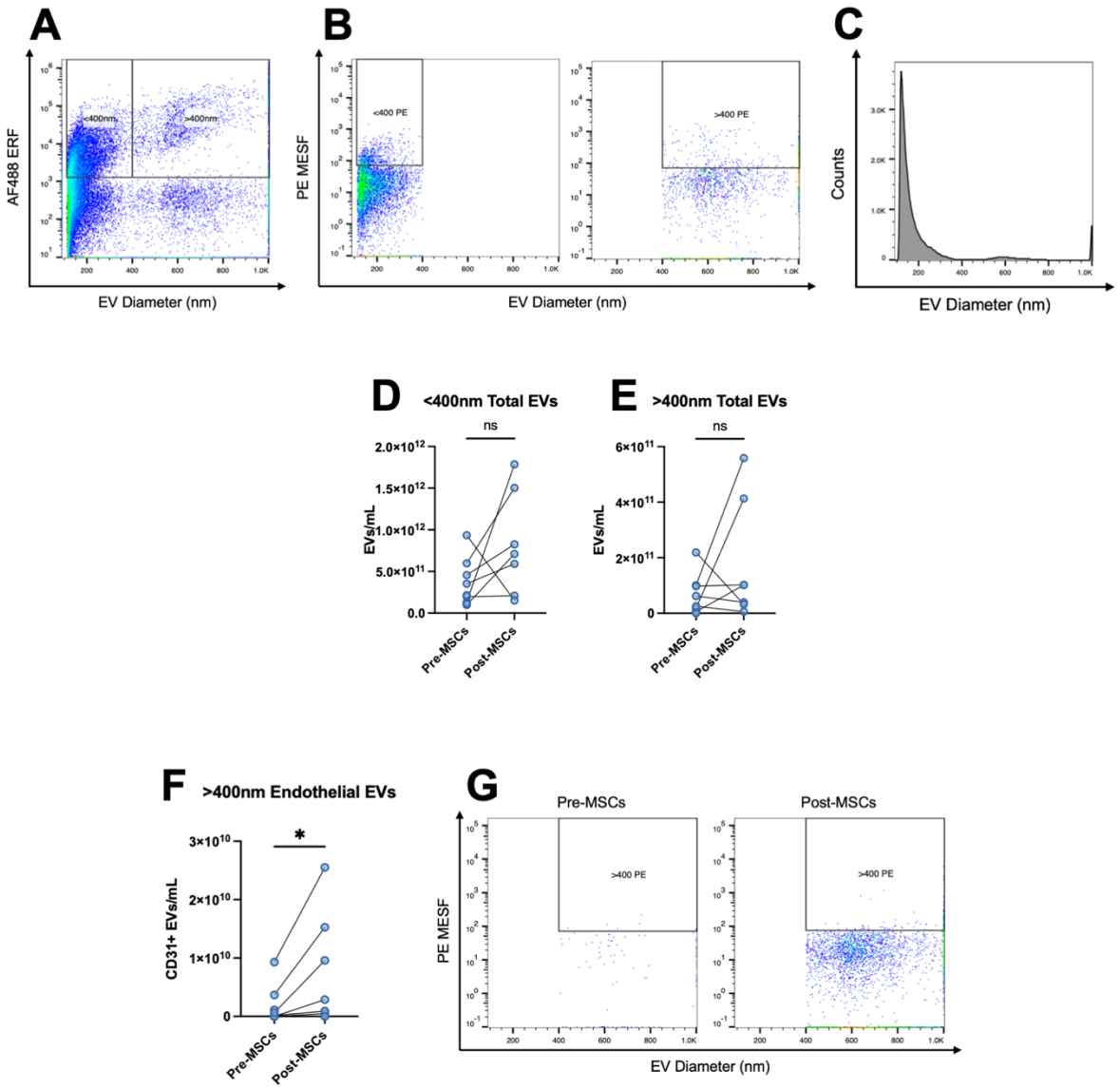

Figure 10. Nanoflow cytometric evaluation of TA-EVs by size. (**A**) Representative flow cytometry plot showing that total TA-EVs form two populations: one population from 110 nm to just under 400 nm, and one from around 500 nm to 1000 nm. (**B**) Representative CD45 staining of TA-EVs gated according to the total EV size separation. (**C**) Histogram of total EVs demonstrating that the majority of EVs are below 400 nm, whereas the larger population comprises a small portion of EVs. (**D**) Total EVs less than 400 nm compared before and after treatment with MSCs. Wilcoxon matched-pairs signed rank test, n=7, $P > 0.05$ (**E**) Total EVs larger than 400 nm compared before and after treatment with MSCs. Wilcoxon matched-pairs signed rank test, n=7, $P > 0.05$ (**F**) >400 nm endothelial (CD31+) EVs compared before and after treatment with MSCs. Wilcoxon matched-pairs signed rank test, n=7, $P < 0.05$ (**G**) Representative flow cytometry plot showing >400 nm endothelial EVs from the same patient before and after treatment with MSCs. *AF488 ERF, AlexaFluor 488 equivalent reference fluorophore; PE MESF, phycoerythrin molecules of equivalent soluble fluorophore; MSC, mesenchymal stromal cell; TA-EV, tracheal aspirate extracellular vesicle.*

4.5 Abundant proteins in TA-EVs are related to neutrophils and AT2 cells

Mass spectrometry was carried out on 3 biological replicates of TA-EVs to better understand their proteome. Common EV markers detected in each sample included CD9, CD63, CD81, TSG101, PDCD6IP, flotillin-1 and flotillin-2, suggesting that enrichment of EVs from TA was successful. However, we did also detect proteins associated with lipoproteins (e.g., apolipoprotein C-1), protein aggregates (e.g, immunoglobulins), the nucleus (e.g., histones), the endoplasmic reticulum or Golgi apparatus (e.g., calnexin) and biofluid-derived corona proteins (e.g., albumin). While these proteins may not be contaminants to TA-EVs, their abundance overshadows that of less abundant proteins, indicating that further purification of the sample may be warranted.

Proteins related to AT2 cells, namely SFTPB, SFTPA2, and DMBT1, and neutrophils, namely DEFA1, S100A9, S100A8, and MPO, were noted in the twenty most abundant proteins, suggesting that EVs from these cells may have been recovered. The top 20 proteins detected in TA-EVs are shown in **Table 5**.

Table 5. List of 20 most abundant proteins in TA-EV.

Uniprot Number	Protein	Protein name	Log2 Max LFQ value		
			Rep 1	Rep 2	Rep 3
P59665	DEFA1	Neutrophil defensin 1	27.35	35.68	38.08
P07988	SFTPB	Pulmonary surfactant-associated protein B	36.29	36.15	36.40
Q16777	H2AC20	Histone H2A type 2-C	36.00	35.46	34.95
P69892	HBG2	Hemoglobin subunit gamma-2	35.51	35.62	35.40
P62805	H4C1	Histone H4	34.75	34.85	36.09
P58876	H2BC5	Histone H2B type 1-D	34.36	34.66	36.18
P69905	HBA2	Hemoglobin subunit alpha	35.62	35.09	35.09
P02768	ALB	Albumin	34.69	35.68	34.80
P06702	S100A9	Protein S100-A9	33.91	35.40	35.27
Q9UGM3-3	DMBT1	Isoform 3 of Deleted in malignant brain tumors 1 protein	34.49	34.80	35.01
P05109	S100A8	Protein S100-A8	33.16	34.85	34.25
Q8IWL1	SFTPA2	Pulmonary surfactant-associated protein A2	34.41	33.62	34.00
P68871	HBB	Hemoglobin subunit beta	34.78	33.52	32.90
Q9Y6R7	FCGBP	IgGFc-binding protein	33.77	34.08	33.78

Q9HC84	MUC5B	Mucin-5B	33.29	33.64	34.25
P02788	LTF	Lactotransferrin	33.64	33.19	33.76
P05164-2	MPO	Isoform H14 of Myeloperoxidase	32.60	33.13	34.13
P60709	ACTB	Actin, cytoplasmic 1	33.51	33.11	32.76
P04264	KRT1	Keratin, type II cytoskeletal 1	32.15	33.21	33.67
Q8TDL5	BPIFB1	BPI fold-containing family B member 1	32.82	32.54	33.41

MaxLFQ, MaxQuant label-free quantification; Rep, replicate.

5. Discussion and future directions

5.1 Discussion

In this work, we have characterized EVs isolated from TA of premature infants before and after they received intravenous MSCs. We also characterized TA-EVs from an observational cohort of infants who were not treated with MSCs. We show that 1) TA from premature infants contains EVs up to 1μM, which vary in concentration; 2) these EVs likely originate from lung epithelium and immune cells; 3) TA-EVs increase following intravenous infusion of MSCs; although 4) we could not identify consistent changes in TA-EV origin following MSC treatment.

Advances in neonatal care have allowed the survival of the smallest premature infants, yet chronic complications of prematurity impact their quality of life. MSCs are currently being tested in early phase clinical trials as potential treatments for BPD, as their pleiotropic effects are expected to reduce inflammation and overcome arrested lung development. The exact ways in which MSCs interact with cells of the premature lung remain uncharacterized. The discovery of EVs as surrogates for cellular alterations in disease has led to an uptick in studies analyzing their molecular cargo (67). We therefore sought to determine if MSC treatment in premature infants changed the proteomic fingerprint of EVs in TA.

EVs in TA have not been extensively studied (see **Section 1.3.3**). We therefore conducted characterization of TA-EVs to establish their size, concentration, protein concentration, and the presence of common EV markers. These characteristics may also provide information on the state of their cell of origin: cellular stress can lead to increased EV secretion (68), and the size of EVs in TA has been found to vary by stage of lung development at birth (78,82). While the relationship between total protein measurement of EVs and disease states is less well understood, this measurement has been associated with diseases such as idiopathic pulmonary fibrosis (108). In our study, NTA demonstrated the presence of particles up to 1 μm in TA. Particle size, concentration, and protein concentration did not vary between

cohorts or timepoints. We did not observe any differences following treatment with MSCs in the HULC-1 cohort. While we did find increased EVs after MSCs with nFC, we suspect that this is due to the staining and detergent used, which increases the specificity of events that we considered to be EVs. We assessed the purity of our TA-EV preparations using mass spectrometry. The detection of single- and multi-pass transmembrane proteins (CD9, major histocompatibility class II protein), along with the presence of cytosolic proteins (TSG101, PDCD6IP, flotillins) provide evidence of an enclosed membranous structure. We did detect proteins characteristic of lipoproteins (apolipoprotein C), the nucleus (histones), and the secretory pathway (calnexin), suggesting that our TA-EV protocol could be further refined to improve the purity. As TA-EVs have not been extensively studied, we were concerned that further purification steps could result in significant EV loss, but our current results suggest that this would not be the case. However, as the field of EV proteomics expands, it is worth noting that there is growing evidence that some so-called "contaminant" proteins may in fact be components of the EV corona (109).

Our main finding was that intravenous infusion of MSCs led to a nearly 3-fold increase in TA-EVs. This finding is interesting as it could be linked directly or indirectly to the MSCs. One possibility is that MSCs travel to the lungs, where they remain for a short period of time, producing EVs that are then accumulated in TA. Our bead-based surface marker analysis of TA-EVs, however, did not reveal the presence of CD105, a known marker of MSCs. Another possibility is that as a response to MSCs, cells of the lung increase their production of EVs, which then end up in TA. This is plausible as even though nFC did not reveal consistent changes in TA-EV cellular origin, MSCs could be producing an effect that is not specific to a certain cell type. In fact, a similar finding was reported in a study that treated chronic stroke patients with intravenous MSCs, where a 5-fold increase in circulating EVs within 24 hours of treatment was observed (110). To our knowledge, this is the only such study to have used EVs to evaluate the treatment effect of MSCs in any disease. Further studies should investigate the biodistribution of both endogenous and MSC derived EVs following MSC treatment to clarify these findings. Furthermore, in our pilot analysis of urine EVs (uEV), we did not observe an increase in uEV sampled at the same time as

TA-EV (**Appendix C**), which speaks to mechanisms of EV clearance and biodistribution that are not yet clear.

Taking into account the clear separation of TA-EVs into two populations (one <400 nm and one >400 nm), we re-gated and analyzed the data using the same method. We did not observe any changes in total EVs in the HULC-1 Post-MSC group from either population, suggesting that both contribute to the increase. Surprisingly, we did note a modest increase in endothelial (CD31+) EVs between 400-1000 nm following administration of MSCs, which was not seen in the HULC-Obs group Post samples. Larger endothelial derived EVs have typically been associated with endothelial cell injury, dysfunction, and inflammation (111,112). This observation may be a reflection of MSCs interacting with lung endothelium, or could be an initial moderate inflammatory response of endothelium, given the interaction of MSCs with immune cells. Further studies are required to explain this finding.

To better understand the cellular origins of TA-EVs in premature infants, we used a multiplexed bead-based flow cytometric approach. This experiment revealed strong detection of CD326, HLA-DRDPDQ, CD133 and CD24. CD326 is an epithelial cell marker, and its detection on TA-EVs is expected due to the proximal and distal airways being composed of various types of epithelial cells. HLA-DRDPDQ is a marker of antigen presenting cells in adult and fetal lung, such as monocytes, dendritic cells and B cells, which are frequently present in TA. Cellular expression of CD133 and CD24 in the premature, developing and fetal lung is less clear. CD24 is expressed by B cells, and in fetal lung, by ciliated epithelial cells. CD133 is used as a marker of stem cells, and, like CD24, is expressed in fetal lung ciliated epithelial cells (113,114). Ransom *et al*. used a similar experimental approach comparing TA-EVs from premature infants born either in the late canalicular or saccular stage of lung development (82). They detected strong expression of CD326, HLA-DRDPDQ and CD133 in their samples, although CD24 was only modestly detected. They did however find that infants born in the late canalicular stage had higher detection of CD24 compared to those born in the saccular stage, and that this correlated with

development of BPD. This suggests that CD24 may have functional involvement in the pathogenesis of the condition, however this remains to be investigated.

Our mass spectrometry experiment revealed the presence of proteins produced by epithelial and immune cells. DEFA1, S100A9, S100A8 and MPO are produced by lung neutrophils (115), and their abundance provides evidence that neutrophil-derived TA-EVs may be major contributors to the TA-EV pool. Indeed, a previous study established the presence of pathogenic neutrophil derived TA-EVs in infants with BPD (81), and neutrophils have been identified by several studies as key players in the pathophysiology of BPD (20,116). AT2-specific proteins SFTPB and SFTPA2 (115) were also abundant in our samples, indicating that some EVs by these cells may have been captured in our preparations. Alterations in AT2 morphology and function have been described in BPD (28,29), so this result is promising for the future study of EVs derived from these cell types. Further mass spectrometric analysis should be conducted to better describe the proteome of TA-EVs and map the cellular origin of these EVs.

We found a high degree of variability in TA-EV measurements, and, for TA-EVs from specific cellular origins, no consistent changes between timepoints were observed for either the treated or the observational cohort. There are several possible explanations for this result. First, it is possible that the timing of the post-MSC sampling may have occurred too soon to observe a response in TA-EVs. In clinical trials of MSCs for BPD, none of the TA cytokines and growth factors measured at day 3 post-MSCs showed any significant differences compared to pre-treatment levels. Differences were only observed as of day 7 post-MSCs (45). Therefore, measurement of TA-EVs at post-MSC day 7 may have shown more consistent results. Second, the clinical course and incidence of complications of prematurity of each infant varies, and this may affect EV release by certain cell types. Given what we know about injurious stimuli and EV release, it is likely that factors beyond treatment with MSCs, like ventilation and FiO_2, impact the rate of EV production. However, the effect of other factors such as treatment with corticosteroids or antibiotics are less well understood. Furthermore, due the small sample size in this study, it is difficult to draw conclusions on the impact of other factors on EV production. While prenatal

characteristics such as preeclampsia may also impact EVs in infants (117), these were fairly homogenous in our cohorts. Third, the process of tracheal aspiration is not standardized and is prone to variable dilution factors, which may affect our interpretation of EV concentrations (118,119). This may be mitigated in the future by having a single operator performing the sample collection, or by identification of an analyte to which TA-EVs may be normalized.

Technical factors may also have impacted our ability to identify differences in EV cellular origin before and after infants received MSCs. The antigen density of EVs is significantly lower than that of cells: even very abundant EV markers may only have a brightness of around 1000 MESF (120). It is therefore important to choose abundant markers to be able to distinguish EVs from the background. The markers we chose have been used in studies exploring EVs from BALF, however the patient population of these studies was adults. While these markers are expressed in the developing lung, it is possible that there are more highly expressed markers that we could evaluate. Indeed, bead-based surface marker expression showed high detection of CD24 and CD133. We did not use these markers for nFC since we were interested in the cell of origin of EVs, and those markers have more ambiguous cellular expression compared to CD45 or CD326. It is also of note that CD45, while not detected very highly in the bead array, was very well detected by nFC. This finding may warrant the use of positive controls to clarify the inconsistency.

5.2 Future directions

TA-EVs show potential for understanding the interactions between MSCs and the premature lung and this study has provided important details and questions for future work. To better understand these interactions, it would be beneficial to establish basic knowledge of TA-EVs in a large cohort of premature infants receiving standard care. While we attempted to address this by using an observational cohort of infants, we observed variation in nFC measurements that was unexpected. Indeed, preliminary results of circulating EVs in premature infants showed significant increases in platelet EVs between DOL 1 and DOL 3, demonstrating that development and adaptation to extrauterine life also influence EV

measurements (121). Furthermore, technical variation in TA sampling could affect the number of EVs recovered in each sample. The identification of these limitations warrants an observational study of repeated TA sampling by an individual operator to better understand how the clinical course of a premature infant affects EV release, including how specific procedures (for example, surgery), and complications of prematurity (for example, pulmonary hemorrhage), affect TA-EVs.

Another avenue to explore may be through the use of in vitro models. While these models do not replicate the complexity and pathophysiology of infants with BPD, they do offer a more controlled environment to study EVs released from specific cell types of the lung, as well as how they interact with other cell types to effect change. Cell culture of specific lung cell types may be useful to learn about the proteome and transcriptome of these EVs, allowing for better mapping of cellular origin when studying complex biofluids like TA. This may be especially useful for the identification of EVs that are more difficult to detect, such as those released from AT2 cells, which lack a specific cell surface marker. Co-culture models may improve our understanding of EV secretion, uptake and clearance between different cell types. Organoid models further mimic the in vivo environment, which may provide more accurate answers to these questions. Organoids have been used to understand the role of EVs in kidney, eye, and brain development, revealing dynamic temporal changes in secretion, composition, and uptake of EVs (122–124). There is also the opportunity to explore different conditions mimicking the environment of the premature lung in vitro, such as in hyperoxia and cyclic stretch, as well as directly evaluating the effect of MSCs on cell types.

Furthermore, bulk RNA sequencing of TA-EVs could be another way to learn more about the therapeutic effect of MSCs in the lung. As previously discussed, RNAs, in particular miRNAs, have been the focus of many EV studies of BPD as they influence the phenotype of the recipient cell. Comparing miRNAs pre- and post-MSC treatment would be a feasible experiment, and the existing literature, while limited to blood-derived EVs, would be useful to guide the analysis and interpretation of the results. Indeed, when studying circulating EVs in response to MSC treatment for chronic stroke, Bang *et al.*

found increased expression of miRNAs related to neurogenesis in the treatment group compared to the control within 24 hours of treatment (110). miRNA is therefore worth exploring to check for early signs of MSC therapeutic effect.

6. Conclusion

To conclude, this thesis explored TA-EVs from premature infants as potential markers of MSC treatment effect. We primarily relied on a nFC approach to evaluate changes in EVs of different cellular origins after MSC treatment, and complemented this approach with NTA, TEM, bead-based flow cytometry and proteomics. We show that this is a robust method that is feasible to use on clinical TA samples. Future work will focus on a better understanding of TA-EVs from premature infants at different timepoints.

7. References

1. Northway WH, Rosan RC, Porter DY. Pulmonary Disease Following Respirator Therapy of Hyaline-Membrane Disease: Bronchopulmonary Dysplasia. N Engl J Med. 1967 Feb 16;276(7):357–68.

2. Statistics Canada. Live births, by weeks of gestation [Internet]. Government of Canada; [cited 2025 Jan 22]. Available from: https://www150.statcan.gc.ca/t1/tbl1/en/tv.action?pid=1310042501

3. 2023 CNN Annual Report [Internet]. 2023. Available from: https://www.canadianneonatalnetwork.org/portal/Portals/0/Annual%20Reports/2023%20CNN%20Annual%20Report.pdf

4. Stoll BJ, Hansen NI, Bell EF, Walsh MC, Carlo WA, Shankaran S, et al. Trends in care practices, morbidity, and mortality of extremely preterm Neonates, 1993-2012. JAMA - Journal of the American Medical Association. 2015 Sep 8;314(10):1039–51.

5. Lapcharoensap W, Gage SC, Kan P, Profit J, Shaw GM, Gould JB, et al. Hospital Variation and Risk Factors for Bronchopulmonary Dysplasia in a Population-Based Cohort. JAMA Pediatr. 2015 Feb 2;169(2):e143676.

6. Thébaud B, Goss KN, Laughon M, Whitsett JA, Abman SH, Steinhorn RH, et al. Bronchopulmonary dysplasia. Nature Reviews Disease Primers. 2019 Nov 14;5(1):78.

7. Pierro M, Van Mechelen K, van Westering-Kroon E, Villamor-Martínez E, Villamor E. Endotypes of Prematurity and Phenotypes of Bronchopulmonary Dysplasia: Toward Personalized Neonatology. Journal of Personalized Medicine. 2022 May 1;12(5).

8. Schittny JC. Development of the lung. Cell Tissue Res. 2017 Mar;367(3):427–44.

9. Jones R, Capen DE, Reid L. Pulmonary vascular development. In: The Lung [Internet]. Elsevier; 2025 [cited 2025 Mar 1]. p. 71–110. Available from: https://linkinghub.elsevier.com/retrieve/pii/B9780323918244000290

10. Narayanan M, Owers-Bradley J, Beardsmore CS, Mada M, Ball I, Garipov R, et al. Alveolarization Continues during Childhood and Adolescence. Am J Respir Crit Care Med. 2012 Jan 15;185(2):186–91.

11. Bhatt AJ, Pryhuber GS, Huyck H, Watkins RH, Metlay LA, Maniscalco WM. Disrupted Pulmonary Vasculature and Decreased Vascular Endothelial Growth Factor, Flt-1, and TIE-2 in Human Infants Dying with Bronchopulmonary Dysplasia. Am J Respir Crit Care Med. 2001 Nov 15;164(10):1971–80.

12. Morrow LA, Wagner BD, Ingram DA, Poindexter BB, Schibler K, Cotten CM, et al. Antenatal Determinants of Bronchopulmonary Dysplasia and Late Respiratory Disease in Preterm Infants. Am J Respir Crit Care Med. 2017 Aug 1;196(3):364–74.

13. Lal MK, Manktelow BN, Draper ES, Field DJ. Chronic Lung Disease of Prematurity and Intrauterine Growth Retardation: A Population-Based Study. Pediatrics. 2003 Mar 1;111(3):483–7.

14. Bose C, Van Marter LJ, Laughon M, O'Shea TM, Allred EN, Karna P, et al. Fetal Growth Restriction and Chronic Lung Disease Among Infants Born Before the 28th Week of Gestation. Pediatrics. 2009 Sep 1;124(3):e450–8.

15. Keller RL, Feng R, DeMauro SB, Ferkol T, Hardie W, Rogers EE, et al. Bronchopulmonary Dysplasia and Perinatal Characteristics Predict 1-Year Respiratory Outcomes in Newborns Born at Extremely Low Gestational Age: A Prospective Cohort Study. The Journal of Pediatrics. 2017 Aug 1;187:89-97.e3.

16. Villamor-Martinez E, Álvarez-Fuente M, Ghazi AMT, Degraeuwe P, Zimmermann LJI, Kramer BW, et al. Association of Chorioamnionitis With Bronchopulmonary Dysplasia Among Preterm Infants: A Systematic Review, Meta-analysis, and Metaregression. JAMA Network Open. 2019 Nov 6;2(11):e1914611.

17. Salimi U, Dummula K, Tucker MH, Dela Cruz CS, Sampath V. Postnatal Sepsis and Bronchopulmonary Dysplasia in Premature Infants: Mechanistic Insights into "New BPD." Am J Respir Cell Mol Biol. 2022 Feb;66(2):137–45.

18. Hilgendorff A, Parai K, Ertsey R, Jain N, Navarro EF, Peterson JL, et al. Inhibiting lung elastase activity enables lung growth in mechanically ventilated newborn mice. American Journal of Respiratory and Critical Care Medicine. 2011 Sep 1;184(5):537–46.

19. Heydarian M, Schulz C, Stoeger T, Hilgendorff A. Association of immune cell recruitment and BPD development. Molecular and Cellular Pediatrics. 2022;9(1).

20. Sun L, Zhang M, Jiang J, Liu W, Zhao W, Li F. Neutrophil extracellular traps promote bronchopulmonary dysplasia-like injury in neonatal mice via the WNT/β-catenin pathway. Frontiers in Cellular and Infection Microbiology. 2023;13.

21. Song C, Li H, Li Y, Dai M, Zhang L, Liu S, et al. NETs promote ALI/ARDS inflammation by regulating alveolar macrophage polarization. Experimental Cell Research. 2019 Sep 15;382(2).

22. Janardhan K S. Neutrophil depletion inhibits early and late monocyte/macrophage increase in lung inflammation. Front Biosci. 2006;11(1):1569.

23. Zenri H, Rodriquez-Capote K, McCaig L, Yao LJ, Brackenbury A, Possmayer F, et al. Hyperoxia exposure impairs surfactant function and metabolism: Critical Care Medicine. 2004 May;32(5):1155–60.

24. Sies H, Berndt C, Jones DP. Oxidative Stress. Annual Review of Biochemistry. 2017 Jun 20;86(Volume 86, 2017):715–48.

25. Davis JM, Auten RL. Maturation of the antioxidant system and the effects on preterm birth. Seminars in Fetal and Neonatal Medicine. 2010 Aug 1;15(4):191–5.

26. Georgeson GD, Szőny BJ, Streitman K, Varga IS, Kovács A, Kovács L, et al. Antioxidant enzyme activities are decreased in preterm infants and in neonates born via caesarean section. European Journal of Obstetrics & Gynecology and Reproductive Biology. 2002 Jul;103(2):136–9.

27. Perrone S, Tataranno ML, Buonocore G. Oxidative Stress and Bronchopulmonary Dysplasia. J Clin Neonatol. 2012;1(3):109–14.

28. Hou A, Fu J, Yang H, Zhu Y, Pan Y, Xu S, et al. Hyperoxia stimulates the transdifferentiation of type II alveolar epithelial cells in newborn rats. American Journal of Physiology - Lung Cellular and Molecular Physiology. 2015;308(9):L861–72.

29. Xia S, Vila Ellis L, Winkley K, Menden H, Mabry SM, Venkatraman A, et al. Neonatal hyperoxia induces activated pulmonary cellular states and sex-dependent transcriptomic changes in a model of experimental bronchopulmonary dysplasia. American journal of physiology Lung cellular and molecular physiology. 2023 Feb 1;324(2):L123–40.

30. Dylag AM, Misra RS, Bandyopadhyay G, Poole C, Huyck HL, Jehrio MG, et al. New insights into the natural history of bronchopulmonary dysplasia from proteomics and multiplexed immunohistochemistry. American journal of physiology Lung cellular and molecular physiology. 2023 Oct 1;325(4):L419–33.

31. Vadivel A, Abozaid S, Van Haaften T, Sawicka M, Eaton F, Chen M, et al. Adrenomedullin promotes lung angiogenesis, alveolar development, and repair. American Journal of Respiratory Cell and Molecular Biology. 2010 Aug 1;43(2):152–60.

32. Wood NS, Marlow N, Costeloe K, Gibson AT, Wilkinson AR. Neurologic and Developmental Disability after Extremely Preterm Birth. New England Journal of Medicine. 2000 Aug 10;343(6):378–84.

33. Blencowe H, Lawn JE, Vazquez T, Fielder A, Gilbert C. Preterm-associated visual impairment and estimates of retinopathy of prematurity at regional and global levels for 2010. Pediatr Res. 2013 Dec;74(1):35–49.

34. Crump C, Sundquist K, Sundquist J, Winkleby MA. Gestational Age at Birth and Mortality in Young Adulthood. JAMA. 2011 Sep 21;306(11):1233–40.

35. Öhrneman H, Lindström F, Hagman C, Petersson Sjögren M, Rissler J, Wollmer P, et al. Enlarged airspaces in the distal lung in adolescents born very preterm as measured by aerosol. BMJ Open Resp Res. 2024 Dec;11(1):e002666.

36. Flors L, Mugler JP, Paget-Brown A, Froh DK, De Lange EE, Patrie JT, et al. Hyperpolarized Helium-3 Diffusion-weighted Magnetic Resonance Imaging Detects Abnormalities of Lung Structure in Children With Bronchopulmonary Dysplasia. Journal of Thoracic Imaging. 2017 Sep;32(5):323–32.

37. Wong PM, Lees AN, Louw J, Lee FY, French N, Gain K, et al. Emphysema in young adult survivors of moderate-to-severe bronchopulmonary dysplasia. European Respiratory Journal. 2008 Mar 19;32(2):321–8.

38. Doyle LW, Adams AM, Robertson C, Ranganathan S, Davis NM, Lee KJ, et al. Increasing airway obstruction from 8 to 18 years in extremely preterm/low-birthweight survivors born in the surfactant era. Thorax. 2017 Aug;72(8):712–9.

39. Vrijlandt EJLE, Boezen HM, Gerritsen J, Stremmelaar EF, Duiverman EJ. Respiratory Health in Prematurely Born Preschool Children with and without Bronchopulmonary Dysplasia. The Journal of Pediatrics. 2007 Mar 1;150(3):256–61.

40. Dominici M, Le Blanc K, Mueller I, Slaper-Cortenbach I, Marini FC, Krause DS, et al. Minimal criteria for defining multipotent mesenchymal stromal cells. The International Society for Cellular Therapy position statement. Cytotherapy. 2006;8(4):315–7.

41. Augustine S, Avey MT, Harrison B, Locke T, Ghannad M, Moher D, et al. Mesenchymal Stromal Cell Therapy in Bronchopulmonary Dysplasia: Systematic Review and Meta-Analysis of Preclinical Studies. Stem Cells Translational Medicine. 2017 Dec 1;6(12):2079–93.

42. del Cerro Marín MJ, Ormazabal IG, Gimeno-Navarro A, Álvarez-Fuente M, López-Ortego P, Avila-Alvarez A, et al. Repeated Intravenous Doses Of Human Umbilical Cord-Derived Mesenchymal Stromal Cells For Bronchopulmonary Dysplasia: Results of a Phase 1 Clinical Trial with two-year follow-up. Cytotherapy. 2024;000.

43. Ahn SY, Chang YS, Kim JH, Sung SI, Park WS. Two-Year Follow-Up Outcomes of Premature Infants Enrolled in the Phase I Trial of Mesenchymal Stem Cells Transplantation for Bronchopulmonary Dysplasia. The Journal of Pediatrics. 2017 Jun 1;185:49-54.e2.

44. Powell SB, Silvestri JM. Safety of Intratracheal Administration of Human Umbilical Cord Blood Derived Mesenchymal Stromal Cells in Extremely Low Birth Weight Preterm Infants. The Journal of Pediatrics. 2019 Jul 1;210:209-213.e2.

45. Chang YS, Ahn SY, Yoo HS, Sung SI, Choi SJ, Oh WI, et al. Mesenchymal Stem Cells for Bronchopulmonary Dysplasia: Phase 1 Dose-Escalation Clinical Trial. The Journal of Pediatrics. 2014 May 1;164(5):966-972.e6.

46. Ahn SY, Chang YS, Lee MH, Sung SI, Lee BS, Kim KS, et al. Stem Cells for Bronchopulmonary Dysplasia in Preterm Infants: A Randomized Controlled Phase II Trial. Stem Cells Translational Medicine. 2021 Aug 1;10(8):1129–37.

47. Ahn SY, Chang YS, Lee MH, Sung S, Kim AR, Park WS. Five-year follow-up of phase II trial of stromal cells for bronchopulmonary dysplasia. Thorax. 2023 Nov 1;78(11):1105–10.

48. Pierro M, Ionescu L, Montemurro T, Vadivel A, Weissmann G, Oudit G, et al. Short-term, long-term and paracrine effect of human umbilical cord-derived stem cells in lung injury prevention and repair in experimental bronchopulmonary dysplasia. Thorax. 2013;68(5):475–84.

49. Németh K, Leelahavanichkul A, Yuen PST, Mayer B, Parmelee A, Doi K, et al. Bone marrow stromal cells attenuate sepsis via prostaglandin E2–dependent reprogramming of host macrophages to increase their interleukin-10 production. Nature Medicine. 2009 Jan 21;15(1):42–9.

50. Willis GR, Fernandez-Gonzalez A, Anastas J, Vitali SH, Liu X, Ericsson M, et al. Mesenchymal stromal cell exosomes ameliorate experimental bronchopulmonary dysplasia and restore lung function through macrophage immunomodulation. American Journal of Respiratory and Critical Care Medicine. 2018 Jan 1;197(1):104–16.

51. Wang H, Zheng R, Chen Q, Shao J, Yu J, Hu S. Mesenchymal stem cells microvesicles stabilize endothelial barrier function partly mediated by hepatocyte growth factor (HGF). Stem Cell Research and Therapy. 2017 Dec 29;8(1):211.

52. Ahn SY, Park WS, Kim YE, Sung DK, Sung SI, Ahn JY, et al. Vascular endothelial growth factor mediates the therapeutic efficacy of mesenchymal stem cell-derived extracellular vesicles against neonatal hyperoxic lung injury. Experimental and Molecular Medicine. 2018 Apr 1;50(4).

53. Chang YS, Ahn SY, Jeon HB, Sung DK, Kim ES, Sung SI, et al. Critical role of vascular endothelial growth factor secreted by mesenchymal stem cells in hyperoxic lung injury. American Journal of Respiratory Cell and Molecular Biology. 2014;51(3):391–9.

54. Chaubey S, Thueson S, Ponnalagu D, Alam MA, Gheorghe CP, Aghai Z, et al. Early gestational mesenchymal stem cell secretome attenuates experimental bronchopulmonary dysplasia in part via exosome-associated factor TSG-6. Stem Cell Research and Therapy. 2018 Jun 26;9(1).

55. Willis GR, Reis M, Gheinani AH, Fernandez-Gonzalez A, Taglauer ES, Yeung V, et al. Extracellular Vesicles Protect the Neonatal Lung from Hyperoxic Injury through the Epigenetic and Transcriptomic Reprogramming of Myeloid Cells. American Journal of Respiratory and Critical Care Medicine. 2021;204(12):1418–32.

56. Johnstone RM, Adam M, Hammond JR, Orr L, Turbide C. Vesicle formation during reticulocyte maturation. Association of plasma membrane activities with released vesicles (exosomes). Journal of Biological Chemistry. 1987 Jul;262(19):9412–20.

57. Jeppesen DK, Zhang Q, Coffey RJ. Extracellular vesicles and nanoparticles at a glance. Journal of Cell Science. 2024 Dec 1;137(23):jcs260201.

58. Ostrowski M, Carmo NB, Krumeich S, Fanget I, Raposo G, Savina A, et al. Rab27a and Rab27b control different steps of the exosome secretion pathway. Nat Cell Biol. 2010 Jan;12(1):19–30.

59. Pan BT, Teng K, Wu C, Adam M, Johnstone RM. Electron microscopic evidence for externalization of the transferrin receptor in vesicular form in sheep reticulocytes. The Journal of cell biology. 1985 Sep 1;101(3):942–8.

60. Heijnen HFG, Schiel AE, Fijnheer R, Geuze HJ, Sixma JJ. Activated Platelets Release Two Types of Membrane Vesicles: Microvesicles by Surface Shedding and Exosomes Derived From Exocytosis of Multivesicular Bodies and α-Granules. Blood. 1999 Dec 1;94(11):3791–9.

61. Li B, Antonyak MA, Zhang J, Cerione RA. RhoA triggers a specific signaling pathway that generates transforming microvesicles in cancer cells. Oncogene. 2012 Nov 8;31(45):4740–9.

62. Perez-Hernandez D, Gutiérrez-Vázquez C, Jorge I, López-Martín S, Ursa A, Sánchez-Madrid F, et al. The Intracellular Interactome of Tetraspanin-enriched Microdomains Reveals Their Function as Sorting Machineries toward Exosomes. Journal of Biological Chemistry. 2013 Apr 26;288(17):11649–61.

63. Umeda R, Satouh Y, Takemoto M, Nakada-Nakura Y, Liu K, Yokoyama T, et al. Structural insights into tetraspanin CD9 function. Nat Commun. 2020 Mar 30;11(1):1606.

64. Chanda D, Otoupalova E, Hough KP, Locy ML, Bernard K, Deshane JS, et al. Fibronectin on the surface of extracellular vesicles mediates fibroblast invasion. American Journal of Respiratory Cell and Molecular Biology. 2019 Mar 1;60(3):279–88.

65. Schneider DJ, Speth JM, Penke LR, Wettlaufer SH, Swanson JA, Peters-golden M. Mechanisms and modulation of microvesicle uptake in a model of alveolar cell communication. Journal of Biological Chemistry. 2017;292(51):20897–910.

66. Bourdonnay E, Zasłona Z, Penke LRK, Speth JM, Schneider DJ, Przybranowski S, et al. Transcellular delivery of vesicular SOCS proteins from macrophages to epithelial cells blunts inflammatory signaling. J Exp Med. 2015 May 4;212(5):729–42.

67. Dixson AC, Dawson TR, Di Vizio D, Weaver AM. Context-specific regulation of extracellular vesicle biogenesis and cargo selection. Nat Rev Mol Cell Biol. 2023 Jul;24(7):454–76.

68. Letsiou E, Sammani S, Zhang W, Zhou T, Quijada H, Moreno-Vinasco L, et al. Pathologic mechanical stress and endotoxin exposure increases lung endothelial microparticle shedding. American Journal of Respiratory Cell and Molecular Biology. 2015;52(2):193–204.

69. Mahida RY, Price J, Lugg ST, Li H, Parekh D, Scott A, et al. CD14-positive extracellular vesicles in bronchoalveolar lavage fluid as a new biomarker of acute respiratory distress syndrome. American journal of physiology Lung cellular and molecular physiology. 2022;322(4):L617–24.

70. Wang L, Tang Y, Tang J, Liu X, Zi S, Li S, et al. Endothelial cell-derived extracellular vesicles expressing surface VCAM1 promote sepsis-related acute lung injury by targeting and reprogramming monocytes. Journal of extracellular vesicles. 2024;13(3):e12423.

71. Soni S, Garner JL, O'Dea KP, Koh M, Finney L, Tirlapur N, et al. Intra-alveolar neutrophil-derived microvesicles are associated with disease severity in COPD. American Journal of Physiology - Lung Cellular and Molecular Physiology. 2021;320(1):L73–83.

72. Bazzan E, Radu CM, Tinè M, Neri T, Biondini D, Semenzato U, et al. Microvesicles in bronchoalveolar lavage as a potential biomarker of COPD. American journal of physiology Lung cellular and molecular physiology. 2021 Feb 1;320(2):L241–5.

73. d'Alessandro M, Soccio P, Bergantini L, Cameli P, Scioscia G, Barbaro MPF, et al. Extracellular vesicle surface signatures in ipf patients: A multiplex bead-based flow cytometry approach. Cells. 2021;10(5):1–12.

74. Lopriore E. The total volume of blood in an extremely preterm neonate is about the size of a double espresso. Acta Paediatrica. 2023;112(12):2458–9.

75. Aladangady N, McHugh S, Aitchison TC, Wardrop CAJ, Holland BM. Infants' Blood Volume in a Controlled Trial of Placental Transfusion at Preterm Delivery. Pediatrics. 2006 Jan 1;117(1):93–8.

76. Counsilman CE, Heeger LE, Tan R, Bekker V, Zwaginga JJ, te Pas AB, et al. Iatrogenic blood loss in extreme preterm infants due to frequent laboratory tests and procedures. The Journal of Maternal-Fetal & Neonatal Medicine. 2021 Aug 18;34(16):2660–5.

77. Veerappan A, Thompson M, Savage AR, Silverman ML, Chan WS, Sung B, et al. Mast cells and exosomes in hyperoxia-induced neonatal lung disease. American Journal of Physiology - Lung Cellular and Molecular Physiology. 2016;310(11):L1218–32.

78. Lal CV, Olave N, Travers C, Rezonzew G, Dolma K, Simpson A, et al. Exosomal microRNA predicts and protects against severe bronchopulmonary dysplasia in extremely premature infants. JCI insight. 2018;3(5).

79. Rajan S, Panzade G, Srivastava A, Shankar K, Pandey R, Kumar D, et al. miR-876-3p regulates glucose homeostasis and insulin sensitivity by targeting adiponectin. 2018 Oct 1;

80. Yang F, Zhao WJ, Jia CL, Li XK, Wang Q, Chen ZL, et al. MicroRNA-876-3p functions as a tumor suppressor gene and correlates with cell metastasis in pancreatic adenocarcinoma via targeting JAG2. Am J Cancer Res. 2018 Apr 1;8(4):636–49.

81. Genschmer KR, Russell DW, Lal C, Szul T, Bratcher PE, Noerager BD, et al. Activated PMN Exosomes: Pathogenic Entities Causing Matrix Destruction and Disease in the Lung. Cell. 2019;176(1–2):113-126.e15.

82. Ransom MA, Bunn KE, Negretti NM, Jetter CS, Bressman ZJ, Sucre JMS, et al. Developmental Trajectory of Extracellular Vesicles Characteristics from the Lungs of Preterm Infants. American journal of physiology Lung cellular and molecular physiology. 2023;(November 2022).

83. Iosef C, Alastalo TP, Hou Y, Chen C, Adams ES, Lyu SC, et al. Inhibiting NF-κB in the developing lung disrupts angiogenesis and alveolarization. American Journal of Physiology-Lung Cellular and Molecular Physiology. 2012 May 15;302(10):L1023–36.

84. Wang X, Yao F, Yang L, Han D, Zeng Y, Huang Z, et al. Macrophage extracellular vesicle-packaged miR-23a-3p impairs maintenance and angiogenic capacity of human endothelial progenitor cells in neonatal hyperoxia-induced lung injury. Stem Cell Research & Therapy. 2024 Sep 11;15(1):295.

85. Li J, Zhao Y, Lu Y, Ritchie W, Grau G, Vadas MA, et al. The Poly-cistronic miR-23-27-24 Complexes Target Endothelial Cell Junctions: Differential Functional and Molecular Effects of miR-23a and miR-23b. Mol Ther Nucleic Acids. 2016 Aug 1;5(8):e354.

86. Zhou Q, Gallagher R, Ufret-Vincenty R, Li X, Olson EN, Wang S. Regulation of angiogenesis and choroidal neovascularization by members of microRNA-23~27~24 clusters. Proc Natl Acad Sci U S A. 2011 May 1;108(20):8287–92.

87. Go H, Maeda H, Miyazaki K, Maeda R, Kume Y, Namba F, et al. Extracellular vesicle miRNA-21 is a potential biomarker for predicting chronic lung disease in premature infants. Am J Physiol Lung Cell Mol Physiol. 2020;318:845–51.

88. Jenike AE, Halushka MK. miR-21: a non-specific biomarker of all maladies. Biomarker Research. 2021 Mar 12;9(1):18.

89. Makiguchi T, Yamada M, Yoshioka Y, Sugiura H, Koarai A, Chiba S, et al. Serum extracellular vesicular miR-21-5p is a predictor of the prognosis in idiopathic pulmonary fibrosis. Respir Res. 2016 Sep 5;17(1):110.

90. Abd-El-Fattah AA, Sadik NAH, Shaker OG, Aboulftouh ML. Differential MicroRNAs Expression in Serum of Patients with Lung Cancer, Pulmonary Tuberculosis, and Pneumonia. Cell Biochem Biophys. 2013 Dec 1;67(3):875–84.

91. Zhong XQ, Yan Q, Chen ZG, Jia CH, Li XH, Liang ZY, et al. Umbilical Cord Blood-Derived Exosomes From Very Preterm Infants With Bronchopulmonary Dysplasia Impaired Endothelial Angiogenesis: Roles of Exosomal MicroRNAs. Frontiers in Cell and Developmental Biology. 2021;9(March):1–14.

92. Zhang Y, Qiao X, Liu L, Han W, Liu Q, Wang Y, et al. Long noncoding RNA MAGI2-AS3 regulates the H2O2 level and cell senescence via HSPA8. Redox Biology. 2022 Aug;54:102383.

93. Zhong X qi, Hao T fang, Zhu Q jiong, Zheng J, Zheng M fei, Li X hong, et al. Umbilical cord blood exosomes from very preterm infants with bronchopulmonary dysplasia aggravate lung injury in mice. Scientific Reports. 2023 Dec 1;13(1).

94. Starke N, Challa NVD, Yuan H, Chen S, Duncan MR, Cabrera Ranaldi ED, et al. Extracellular Vesicle ASC: A Novel Mediator for Lung-Brain Axis in Preterm Brain Injury. Am J Respir Cell Mol Biol. 2024 Jul 3;rcmb.2023-0402OC.

95. Ali A, Zambrano R, Duncan MR, Chen S, Luo S, Yuan H, et al. Hyperoxia-activated circulating extracellular vesicles induce lung and brain injury in neonatal rats. Scientific Reports. 2021 Dec 1;11(1).

96. Dapaah-Siakwan F, Zambrano R, Luo S, Duncan MR, Kerr N, Donda K, et al. Caspase-1 Inhibition Attenuates Hyperoxia-induced Lung and Brain Injury in Neonatal Mice. Am J Respir Cell Mol Biol. 2019 Sep;61(3):341–54.

97. Olave NC, Halloran B, Ambalavanan N. FGF2 is Secreted in Extracellular Vesicles from Lung Cells. American Journal of Physiology-Lung Cellular and Molecular Physiology. 2024 Jul 16;ajplung.00225.2023.

98. Van Der Pol E, Gemert MJCV, Sturk A, Nieuwland R, Leeuwen TGV. Single vs. swarm detection of microparticles and exosomes by flow cytometry. Journal of Thrombosis and Haemostasis. 2012 May 1;10(5):919–30.

99. Libregts SFWM, Arkesteijn GJA, Németh A, Hoen ENMN 't, Wauben MHM. Flow cytometric analysis of extracellular vesicle subsets in plasma: impact of swarm by particles of non-interest. Journal of Thrombosis and Haemostasis. 2018 Jul 1;16(7):1423–36.

100. Inglis HC, Danesh A, Shah A, Lacroix J, Spinella PC, Norris PJ. Techniques to improve detection and analysis of extracellular vesicles using flow cytometry. Cytometry Part A. 2015;87(11):1052–63.

101. Welsh JA, Van Der Pol E, Arkesteijn GJA, Bremer M, Brisson A, Coumans F, et al. MIFlowCyt-EV: a framework for standardized reporting of extracellular vesicle flow cytometry experiments. Journal of Extracellular Vesicles. 2020;9(1).

102. Gasecka A, Böing AN, Filipiak KJ, Nieuwland R. Platelet extracellular vesicles as biomarkers for arterial thrombosis. Platelets. 2017 Apr 3;28(3):228–34.

103. Costantini TW, Park DJ, Johnston W, Nakatsutsumi K, Kezios J, Weaver JL, et al. A Heterogenous Population of Extracellular Vesicles Mobilize to the Alveoli Post-Injury. Journal of Trauma and Acute Care Surgery. 2023 Oct 26;

104. Kong AT, Leprevost FV, Avtonomov DM, Mellacheruvu D, Nesvizhskii AI. MSFragger: ultrafast and comprehensive peptide identification in mass spectrometry–based proteomics. Nat Methods. 2017 May;14(5):513–20.

105. Welsh JA, Killingsworth B, Kepley J, Traynor T, Cook S, Savage J, et al. MPAPASS software enables stitched multiplex, multidimensional EV repertoire analysis and a standard framework for reporting bead-based assays. Cell Reports Methods. 2022;2(1).

106. Welsh JA, Horak P, Wilkinson JS, Ford VJ, Jones JC, Smith D, et al. FCMPASS Software Aids Extracellular Vesicle Light Scatter Standardization. Cytometry Part A. 2020;97(6):569–81.

107. Welsh JA, Goberdhan DCI, O'Driscoll L, Buzas EI, Blenkiron C, Bussolati B, et al. Minimal information for studies of extracellular vesicles (MISEV2023): From basic to advanced approaches. Journal of Extracellular Vesicles. 2024 Feb 7;13(2).

108. Martin-Medina A, Lehmann M, Burgy O, Hermann S, Baarsma HA, Wagner DE, et al. Increased extracellular vesicles mediate WNT5A signaling in idiopathic pulmonary fibrosis. American Journal of Respiratory and Critical Care Medicine. 2018;198(12):1527–38.

109. Tóth EÁ, Turiák L, Visnovitz T, Cserép C, Mázló A, Sódar BW, et al. Formation of a protein corona on the surface of extracellular vesicles in blood plasma. Journal of Extracellular Vesicles. 2021;10(11):e12140.

110. Bang OY, Kim EH, Cho YH, Oh MJ, Chung JW, Chang WH, et al. Circulating Extracellular Vesicles in Stroke Patients Treated With Mesenchymal Stem Cells: A Biomarker Analysis of a Randomized Trial. Stroke. 2022 Jul;53(7):2276–86.

111. Amabile N, Heiss C, Real WM, Minasi P, McGlothlin D, Rame EJ, et al. Circulating Endothelial Microparticle Levels Predict Hemodynamic Severity of Pulmonary Hypertension. American Journal of Respiratory and Critical Care Medicine. 2012 Dec 20;

112. Burger D, Schock S, Thompson CS, Montezano AC, Hakim AM, Touyz RM. Microparticles: Biomarkers and beyond. Clinical Science. 2013 Apr;124(7):423–41.

113. He P, Lim K, Sun D, Pett JP, Jeng Q, Polanski K, et al. A human fetal lung cell atlas uncovers proximal-distal gradients of differentiation and key regulators of epithelial fates. Cell. 2022;185(25):4841-4860.e25.

114. Barnes JL, Yoshida M, He P, Worlock KB, Lindeboom RGH, Suo C, et al. Early human lung immune cell development and its role in epithelial cell fate. Sci Immunol. 2023 Dec 22;8(90):eadf9988.

115. Uhlén M, Fagerberg L, Hallström BM, Lindskog C, Oksvold P, Mardinoglu A, et al. Tissue-based map of the human proteome. Science. 2015 Jan 23;347(6220).

116. Speer CP. Inflammation and bronchopulmonary dysplasia: A continuing story. Seminars in Fetal and Neonatal Medicine. 2006 Oct;11(5):354–62.

117. Campello E, Spiezia L, Radu CM, Dhima S, Visentin S, Valle FD, et al. Circulating microparticles in umbilical cord blood in normal pregnancy and pregnancy with preeclampsia. Thrombosis Research. 2015 Aug;136(2):427–31.

118. Rennard SI, Basset G, Lecossier D, O'Donnell KM, Pinkston P, Martin PG, et al. Estimation of volume of epithelial lining fluid recovered by lavage using urea as marker of dilution. Journal of Applied Physiology. 1986 Feb 1;60(2):532–8.

119. Watts CL, Bruce MC. Comparison of secretory component for immunoglobulin A with albumin as reference proteins in tracheal aspirate from preterm infants. The Journal of Pediatrics. 1995 Jul 1;127(1):113–22.

120. Welsh JA, Arkesteijn GJA, Bremer M, Cimorelli M, Dignat-George F, Giebel B, et al. A compendium of single extracellular vesicle flow cytometry. Journal of Extracellular Vesicles. 2023;12(2).

121. O'Reilly D, Egan K, Burke O, Griffiths A, Neary E, Blanco A, et al. The Population of Circulating Extracellular Vesicles Dramatically Alters after Very Premature Delivery- a Previously Unrecognised Postnatal Adaptation Process? Blood. 2018 Nov 29;132(Supplement 1):1129.

122. Ahmad N, Samoylenko A, Abene I, Abdelrady E, Zhyvolozhnyi A, Makieieva O, et al. Generation of novel in vitro flexible kidney organoid model to investigate the role of extracellular vesicles in induction of nephrogenesis. Cell Communication and Signaling. 2023 Dec 18;21(1):358.

123. Zhou J, Flores-Bellver M, Pan J, Benito-Martin A, Shi C, Onwumere O, et al. Human retinal organoids release extracellular vesicles that regulate gene expression in target human retinal progenitor cells. Scientific Reports. 2021;11(1):1–17.

124. Forero A, Pipicelli F, Moser S, Baumann N, Grätz C, Gonzalez Pisfil M, et al. Extracellular vesicle-mediated trafficking of molecular cues during human brain development. Cell Reports. 2024 Oct 22;43(10):114755.

Appendix A

Table A1. MiFlowCyt-EV framework.

Framework Criteria	
1.1 Preanalytical variables conforming to MISEV guidelines.	TA were collected by flushing approximately 1 mL of saline from the suction catheter and collected in a specimen trap. The sample was then placed in a cooler containing an ice pack for transport to the lab. TA was centrifuged 1,500 x g for 10 minutes at 4C, and the supernatant (referred to as "cleared TA") was transferred to a cryovial for storage at -80C. Cleared TA were further prepared once all study samples had been received by the lab. Cleared TA were transferred to ultracentrifugation tubes and ultracentrifuged 100,000 x g for 90 minutes at 4C using an Optima Max Ultracentrifuge (Beckman Coulter) with a TLA 100.3 rotor (Beckman Coulter). The supernatant was removed and stored in case of requirements for future analysis. The pellet (or, in absence of a pellet, a small volume of supernatant) was resuspended in 100 µL of 0.1 µM filtered PBS (hereafter referred to as filtered PBS) and stored in 5 20 µL aliquots. One aliquot was immediately used for nanoparticle tracking analysis (NTA), whereas the other 4 were immediately stored at -80C.
1.2 Experimental design according to MIFlowCyt guidelines.	**1.1 Experimental aim:** characterize EVs isolated from tracheal aspirates of infants enrolled in HULC-1, before and after they received MSCs. **1.2 Keywords:** EV, extracellular vesicle; BPD, bronchopulmonary dysplasia; MSC, mesenchymal stromal cell; TA, tracheal aspirate . **1.3 Variables:** 9 samples were studied from premature infants prior to MSC treatment, and 7 samples were studied after MSC treatment. 20 samples from an observational cohort of untreated premature infants were also studied. There were no demographic differences between the two cohorts.
2.1 Sample staining details	EVs were stained with a combination of CFSE and CMG to determine the concentration of total EVs. 8-point titrations of all reagents were conducted on a pooled TA-EV sample to experimentally determine the optimal concentration. A solution of 1:500 CMG and 20 µM CFSE was added to EVs (volume double that of the staining solution) and incubated for 25 minutes at 37C. This was followed by a two hour incubation at 4C in the dark with phycoerythrin (PE) conjugated antibodies against CD31 (endothelial derived), CD45 (immune derived), CD326 (epithelial derived), CD86 (M1 macrophage derived) and CD206 (M2 macrophage derived) to determine EV cellular origin. See Table 2 for reagents used and final staining concentrations.
2.2 Sample washing details	Samples were not washed due to concerns about EV loss.
2.3 Sample dilution details	Samples were initially diluted 10x for staining. During staining, they were further diluted 2x. Due to the nature of the clinical samples, there was variability in the dilution factor required to avoid swarm detection during acquisition. The acquisition dilution therefore ranged from 2000x to 200,000x. Reported concentrations account for these dilutions as well as the flow rate at which samples were analyzed (10 µL/min)
3.1 Buffer alone controls.	Buffer (0.1 µM filtered PBS) was analyzed at the same time and with the same settings as the samples of interest.

3.2 Buffer with reagent controls.	Buffer with reagent controls were analyzed at the same settings and concentrations as the samples of interest. Due to the number of samples to be analyzed (>400), it was not possible to run this control on the same day as the samples. The median number of events in the FITC+ gate was 1.82E+7 (7.84E+06 - 1.44E+08) and in the PE+ gate 6.00E+5 (IQR 0 - 2.15E+06), which is significantly lower than in stained samples. These events were subtracted from stained events during analysis to correct for possible reagent aggregation. Also see Figure 9J.
3.3 Unstained controls.	Unstained sample controls were analyzed at the same settings and during the same experiment as their respective stained settings. In the FITC+ gate, the median events was 5.4E+8 (IQR 2.7E+8 - 2.72E+9) and in the FITC/PE gate, 0 (IQR 0 - 1.67E+07). These events were subtracted from stained events during analysis to correct for possible reagent aggregation. Also see Figure 9B and C.
3.4 Isotype controls.	Isotype controls were analyzed with the same settings as the stained samples. Due to the number of samples to be analyzed (>400), it was not possible to run this control on the same day as the samples. PE Mouse IgG1k (Biolegend) antibody was used for CD31 (BD), CD45 (Biolegend) and CD206 (Biolegend). PE Mouse IgG2bk (Biolegend) antibody was used for CD326 (Biolegend) and CD86 (Biolegend). For IgG2bk, 4E+06 EV/mL were detected. For IgG1k, 4.4E+07 EV/mL were detected. Also see Figure 9M.
3.5 Single-stained controls.	Single stained controls for all staining reagents were included. Due to the number of samples to be analyzed (>400), it was not possible to run this control on the same day as the samples. Single stained controls were performed on a pooled sample of EVs. Also see Figure 9.
3.6 Procedural controls.	Procedural controls were not used since we did not use any post-staining techniques that may induce artefacts that could be interpreted as EVs.
3.7 Serial dilutions.	Serial dilutions were performed on a subset of samples. Due to the number of samples to be analyzed, it was not possible to conduct serial dilutions on each individual sample. Instead, we used a concentrated and a diluted sample (as measured by nanoparticle tracking analysis) from each cohort. A 10^3.5-fold dilution was created by adding 1 µL stained EVs to 315 µL filtered PBS. Half log dilutions from the starting 10^3.5-fold dilution to 10^6-fold dilution (7 total dilutions). Events, fluorescence intensity and light scatter in standard units were plotted against the dilution factor to determine the optimal range. See Figure 9D-I for fluorescence and scatter signal intensities in standard units.
3.8. Detergent treated EV-samples	Samples were treated with 1% Triton X-100. Events remained in the gate of interest after Triton X-100 ablation however a significant ($P < 0.0001$, n=36, Wilcoxon signed-pairs matched ranks test) reduction in events was observed. Events remaining after Triton X-100 treatment were not considered to be EVs.
4.1 Trigger Channel(s) and Threshold(s).	Detection was triggered using V-SSC. The trigger threshold was 1500 a.u., equivalent to approximately 114 nm (EV diameter in nm, average RI).
4.2 Flow Rate / Volumetric quantification.	A flow rate of 10µL/minute was used.

4.3 Fluorescence Calibration.	Fluorescence calibration was performed on 2 parameters using FCMPASS software (version 4.2.14). Quantum Alexa Fluor® 488 MESF (Cat: 488A; Lot: 16164) was used for FITC calibration to ERF. BD Quantibrite™ PE Phycoerythrin Fluorescence Quantitation Kit (Cat: 340495; Lot: 27504) was used for PE calibration to MESF. FITC and PE regression both showed a high correlation. FITC: R^2 value of 0.99, with a slope of 1.00 and intercept of 0.04. PE: R^2 valu e of 0.99, with a slope of 1.00 and intercept of 1.13.
4.4 Light Scatter Calibration.	Light scatter calibration was implemented using FCMpass software (version 4.2.14). Polystyrene beads ranging from 80-450 nm (ThermoFisher Scientific, Cat: 3080A, 3100A, 3150A, 3200A, 3240A, 3300A, 3350A, 3400A, 3450A; respective Lot: 228748, 204935, 202026, 205131, 226952, 204665, 199283, 203859, 204047).
5.1 EV diameter/surface area/volume approximation.	EV diameter was approximating using CFSE (cytosolic protein dye) and CellMaskGreen (membrane dye).
5.2 EV refractive index approximation.	EV refractive index was approximated using FCMpass software (see section 4.4).
5.3 EV epitope number approximation.	Epitope number was approximated by dividing the median number of PE MESF by the median surface area of the EVs. Since PE is a large molecule, we assumed that the fluorophore to protein ratio was 1:1. The median epitope number was as follows for CD31, CD45, CD326, CD86, and CD206 respectively: 5.34E-5, 2.12E-4, 8.9E-5, 4.23E-5, and 5.09E-5 PE MESF/nm^2.
6.1 Completion of MIFlowCyt checklist.	Checklist was completed. See Appendix B.
6.2 Calibrated channel detection range	Lower limits of calibrated gates were different between samples due to variability between patients. The median lower limit of the fluorescence ranges examined were 1100 AF488 ERF (IQR 1000 – 1200) and 70 PE MESF (IQR 65 – 76.25). Upper limits were 1.6E+6 AF488 ERF and 1.6E+5 PE MESF.
6.3 EV number/concentration.	We have calculated and reported the EV concentration. This was determined by determining the particles per mL (running samples at 10µL/min, so 10µL x 100 = 1mL) and then accounting for staining and acquisition dilutions for each individual sample. We considered EVs to be events between 110-1000 nm, staining positive for the dyes and antibody, and that were sensitive to detergent lysis (1% Triton X-100).
6.4 EV brightness.	EV brightness was assessed using PE MESF and AF488 ERF. The brightness of PE-stained EVs was not different between cohorts and timepoints. The median brightness of EVs stained for CD31, CD45, CD326, CD86, and CD206 was 126 (IQR 107-161), 137 (IQR 126-161), 126 (113-150), 117 (IQR 104-138) and 115 (IQR 101.2-157.8) PE MESF, respectively. The brightness of AF488 did increase significantly from the Pre-MSC to Post-MSC sample in the HULC-1 cohort, in accordance with the increase of EV concentration. The median brightness of membrane-stained EVs was 4731 AF488 ERF (IQR 3417 – 5983).
7.1. Sharing of data to a public repository.	n/a

Appendix B

Table B1. MiFlowCyt framework.

Requirement	
1.1. Purpose	Characterize EVs isolated from tracheal aspirates of infants enrolled in HULC-1, before and after they received MSCs.
1.2. Keywords	EV, extracellular vesicle; BPD, bronchopulmonary dysplasia; MSC, mesenchymal stromal cell; TA, tracheal aspirate
1.3. Experiment variables	9 samples were studied from premature infants prior to MSC treatment, and 7 samples were studied after MSC treatment. 20 samples from an observational cohort of untreated premature infants were also studied. There were no demographic differences between the two cohorts.
1.4. Organization name and address	Ottawa Hospital Research Institute (OHRI) 501 Smyth Rd, Ottawa, ON K1H 8L6
1.5. Primary contact name and email address	Mairead Green
1.6. Date or time period of experiment	Samples were collected in two cohorts: December 2020-September 2021 and March 2023- November 2023. Samples remained frozen at -80 before analysis in March and April 2024.
1.7. Conclusions	Tracheal aspirate EVs (TA-EV) from premature infants increase following intravenous administration of MSCs, although we could not draw conclusions on any of the EVs of specific cellular origin that were tested before and after MSCs.
1.8. Quality control measures	See MiFlowCyt-EV Sections 3-5 for a description of calibration and controls used in this experiment (Appendix A)
2.1.1.1. (2.1.2.1., 2.1.3.1.) Sample description	EVs isolated from tracheal aspirate secretions of premature infants.
2.1.1.2. Biological sample source description	Human premature infants
2.1.1.3. Biological sample source organism description	TA were collected by flushing approximately 1 mL of saline from the suction catheter and collected in a specimen trap. Infants were median 12 (IQR 9.5-20) days of life at baseline sample collection, and 15 (IQR 13-25) at second TA sampling. One cohort of infants were treated with MSCs (as part of HULC-1, NCT04255147). The second sampling occurred 3-4 days after these infants received MSCs.
2.1.2.2. Environmental sample location	n/a
2.3. Sample treatment description	n/a
2.4. Fluorescence reagent(s) description	EV membrane staining was conducted with CFSE (Invitrogen, C34554) and CellMask Green (Invitrogen, C37608). EV phenotyping was conducting using PE-conjugated antibodies: CD31 (BD Biosciences, 555446), CD45 (Biolegend, 304008), CD326 (Biolegend, 324206), CD86 (Biolegend, 305405), and CD206 (Biolegend, 321105). Also see Table 2.
3.1. Instrument manufacturer	Beckman
3.2. Instrument model	CytoFLEX S with 4 lasers. Fluorescence detector configuration: 405-SSC, 405-450/50, 488-525/40, 561-580/30, and 640-670/30 Scatter detector configuration: FSC, 488-SSC, 405-SSC.

3.3. Instrument configuration and settings	Trigger parameter was Violet SSC, with a threshold of 1150 a.u. Gain (a.u) were as follows: FSC-H 20; FSC-A 20; SSC-H 20; SSC-A 20; SSC_1-H 175; SSC_1-A 175; FL5-H 1500; FL5-A 1500; FL7-H 2000; FL7-A 2000.
4.1. List-mode data files	n/a
4.2. Compensation description	n/a
4.3. Data transformation details	Refer to MIFlowCytEV sections 4 and 5 for detailed description of data transformation (Appendix A)
4.4.1. Gate description	Gates were drawn based on each sample's unstained control. A gate for both FITC and PE were drawn, and the PE gate placed under the FITC gate to obtain a gate containing events staining positive for both fluorophores. See Figure 9A for gating strategy.
4.4.2. Gate statistics	Percentage of events was not used as a statistic because the limitations of nFC are such that the full population of events is not resolved by the cytometer. Event counts in the gate were used instead.
4.4.3. Gate boundaries	See Figure 9A for gating strategy and Section 3.11 for a description of the gate boundaries.

Appendix C

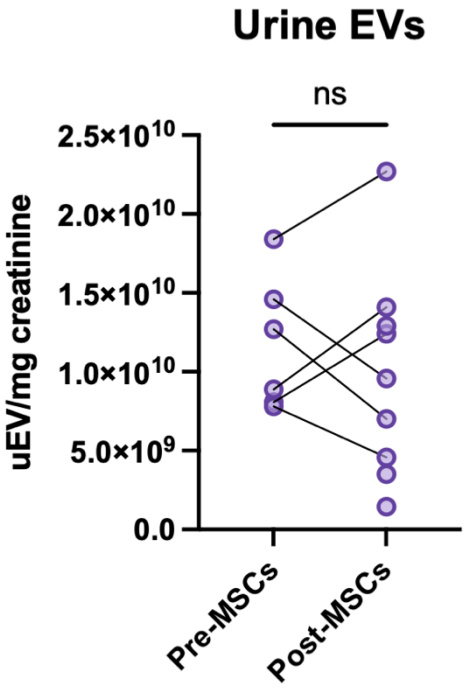

Figure C1. Urine EVs (normalized to urinary creatinine) measured pre- and post-MSCs are not different. *uEV, urine extracellular vesicle; MSC, mesenchymal stromal cell.*